



**UNIVERSIDAD DE INVESTIGACIÓN DE
TECNOLOGÍA EXPERIMENTAL YACHAY**

Escuela de Ciencias de la Tierra, Energía y Ambiente

Title: Volcanogenic Massive Sulfide Deposits from the Macuchi Formation, Ecuador

Trabajo de integración curricular presentado como requisito para la
Obtención del título de Geólogo

Author:

Cristhian Omar Ayala Obando

Tutor:

Dr. Derek James Weller, PhD

Urcuquí, November 2021



SECRETARÍA GENERAL

(Vicerrectorado Académico/Cancillería)
ESCUELA DE CIENCIAS DE LA TIERRA, ENERGÍA Y AMBIENTE
CARRERA DE GEOLOGÍA
ACTA DE DEFENSA No. UITEY-GEO-2022-00001-AD

A los 5 días del mes de enero de 2022, a las 10:00 horas, de manera virtual mediante videoconferencia, y ante el Tribunal Calificador, integrado por los docentes:

Presidente Tribunal de Defensa Dr. GOMEZ PAREDES, JORGE ESTEBAN , Ph.D.

Miembro No Tutor Dr. TORO ALAVA, JORGE EDUARDO , Ph.D.

Tutor Dr. WELLER DEREK JAMES , Ph.D.

El(la) señor(ita) estudiante **AYALA OBANDO, CRISTHIAN OMAR**, con cédula de identidad No. **1723068639**, de la **ESCUELA DE CIENCIAS DE LA TIERRA, ENERGÍA Y AMBIENTE**, de la Carrera de **GEOLOGÍA**, aprobada por el Consejo de Educación Superior (CES), mediante Resolución **RPC-SE-10-No.031-2016**, realiza a través de videoconferencia, la sustentación de su trabajo de titulación denominado: **VOLCANOGENIC MASSIVE SULFIDE DEPOSITS FROM THE MACUCHI FORMATION, ECUADOR**, previa a la obtención del título de **GEÓLOGO/A**.

El citado trabajo de titulación, fue debidamente aprobado por el(los) docente(s):

Tutor Dr. WELLER DEREK JAMES , Ph.D.

Y recibió las observaciones de los otros miembros del Tribunal Calificador, las mismas que han sido incorporadas por el(la) estudiante.

Previamente cumplidos los requisitos legales y reglamentarios, el trabajo de titulación fue sustentado por el(la) estudiante y examinado por los miembros del Tribunal Calificador. Escuchada la sustentación del trabajo de titulación a través de videoconferencia, que integró la exposición de el(la) estudiante sobre el contenido de la misma y las preguntas formuladas por los miembros del Tribunal, se califica la sustentación del trabajo de titulación con las siguientes calificaciones:

Tipo	Docente	Calificación
Tutor	Dr. WELLER DEREK JAMES , Ph.D.	9,4
Presidente Tribunal De Defensa	Dr. GOMEZ PAREDES, JORGE ESTEBAN , Ph.D.	9,6
Miembro Tribunal De Defensa	Dr. TORO ALAVA, JORGE EDUARDO , Ph.D.	9,3

Lo que da un promedio de: **9.4 (Nueve punto Cuatro)**, sobre 10 (diez), equivalente a: **APROBADO**

Para constancia de lo actuado, firman los miembros del Tribunal Calificador, el/la estudiante y el/la secretario ad-hoc.

Certifico que *en cumplimiento del Decreto Ejecutivo 1017 de 16 de marzo de 2020, la defensa de trabajo de titulación (o examen de grado modalidad teórico práctica) se realizó vía virtual, por lo que las firmas de los miembros del Tribunal de Defensa de Grado, constan en forma digital.*

AYALA OBANDO, CRISTHIAN OMAR
Estudiante

Dr. GOMEZ PAREDES, JORGE ESTEBAN , Ph.D.
Presidente Tribunal de Defensa



Firmado electrónicamente por:
JORGE ESTEBAN
GOMEZ PAREDES

Dr. WELLER DEREK JAMES , Ph.D.
Tutor

**DEREK
JAMES
WELLER**

Digitally signed
by DEREK
JAMES WELLER
Date: 2022.01.21
15:09:16 -05'00'

Dr. TORO ALAVA, JORGE EDUARDO , Ph.D.
Miembro No Tutor

TERÁN ROSALES, ANDREA YOLANDA
Secretario Ad-hoc

ANDREA
YOLANDA
TERAN
ROSALES

Firmado
digitalmente por
ANDREA YOLANDA
TERAN ROSALES
Fecha: 2022.01.20
16:03:48 -0500

AUTORÍA

Yo, **CRISTHIAN OMAR AYALA OBANDO**, con cédula de identidad 1723068639, declaro que las ideas, juicios, valoraciones, interpretaciones, consultas bibliográficas, definiciones y conceptualizaciones expuestas en el presente trabajo; así cómo, los procedimientos y herramientas utilizadas en la investigación, son de absoluta responsabilidad de el/la autora (a) del trabajo de integración curricular. Así mismo, me acojo a los reglamentos internos de la Universidad de Investigación de Tecnología Experimental Yachay.

Urcuquí, Noviembre 2021.



Cristhian Omar Ayala Obando

CI: 1723068639

AUTORIZACIÓN DE PUBLICACIÓN

Yo, **Cristhian Omar Ayala Obando**, con cédula de identidad 1723068639, cedo a la Universidad de Investigación y Tecnología Experimental Yachay, los derechos de publicación de la presente obra, sin que deba haber un reconocimiento económico por este concepto. Declaro además que el texto del presente trabajo de titulación no podrá ser cedido a ninguna empresa editorial para su publicación u otros fines, sin contar previamente con la autorización escrita de la Universidad.

Asimismo, autorizo a la Universidad que realice la digitalización y publicación de este trabajo de integración curricular en el repositorio virtual, de conformidad a lo dispuesto en el Art. 144 de la Ley Orgánica de Educación Superior

Urcuquí, Noviembre 2021.



Cristhian Omar Ayala Obando

CI: 1723068639

ACKNOWLEDGEMENTS

I express my gratitude to Yachay Tech University for providing me a quality education, especially to all my professors who have taught me different knowledge that inspired me to learn science. To Azam Soltani as my thesis tutor for giving me the necessary learning bases and the time dedicated to the degree work with the contribution of ideas. To my family for the financial and personal support. To all the professors of carrier of Geology for teaching me to develop new ideas, solve doubts and for everything they gave me. In the same way, I thank my friends and colleagues who accompanied me in this professional training.

RESUMEN

La Formación Macuchi aflora en la zona centro-norte de la cordillera Occidental del Ecuador, albergando depósitos volcanogénicos masivos de sulfuros (VMS) que incluyen: El Domo, La Plata y Macuchi. Este documento presenta una revisión bibliográfica que incluye la geología de los depósitos VMS de Macuchi, así como los procesos fisicoquímicos que presenta el Au en estos depósitos. Los factores que controlan la formación de los depósitos VMS de Macuchi incluyen a) sistemas de fallas trans-corticales (Chimbo-Toachi y Pallantanga), b) compresión oblicua de la placa de Nazca en el norte de los Andes, y c) hundimiento y alta deformación en los bloques acumulados donde se formaron los depósitos. Se sugiere que los depósitos VMS de Macuchi sean bimodales del tipo Noranda / Koruko. La alta deformación en La Plata y la relativa ausencia de deformación en El Domo es consistente con el modelo de compresión oblicua que permitió la mineralización dentro de las cuencas de separación (pull-apart) de la formación Macuchi durante el intervalo Paleoceno-Eoceno. La Plata se clasifica como un depósito VMS rico en Au, con una ley de 12,9g / t Au, mientras que El Domo es un depósito VMS normal, con una ley de 2,99g / t Au. La Formación Macuchi está potencialmente bajo exploración para más ocurrencias de sistemas de mineralización de VMS, por lo tanto, esta sinapsis ayudará al entendimiento de la génesis mineral y la exploración regional para depósitos VMS en esta área.

Palabras clave: Formación Macuchi, Depósito El Domo, Depósito La Plata, VMS Rico-Au, Cordillera Occidental, Ecuador.

ABSTRACT

The Macuchi Formation outcrops in the north-central zone of the Western cordillera of Ecuador, hosting volcanogenic massive sulfide (VMS) deposits including: El Domo, La Plata, and Macuchi. This document presents a bibliographic review including the geology of the Macuchi VMS deposits, as well as the physicochemical processes of Au occurrence in these deposits. The factors that control the formation of the Macuchi's VMS deposits include a) trans-crustal fault systems (Chimbo-Toachi and Pallantanga), b) oblique compression of the Nazca plate in the north of the Andes, and c) subsidence and high deformation in the accumulated blocks where the deposits were formed. The Macuchi VMS deposits are suggested to be bimodal Noranda/Koruko type in origin. The high deformation at La Plata and the relative absence of deformation at El Domo is consistent with the oblique compression model that allowed mineralizations within the Macuchi Formation pull-apart basins during the Paleocene-Eocene interval. La Plata is classified as an Au rich-VMS deposit with a grade of 12.9g / t Au, while El Domo is a normal VMS deposit, having a grade of 2.99g / t Au. The Macuchi Formation is potentially under exploration for more occurrences of VMS mineralization systems, hence this synopsis will help in the understanding of the ore-genesis and regional exploration for VMS deposits in this area.

Key words: Macuchi Formation, El Domo deposit, La Plata deposit, Au-rich VMS, Western Cordillera, Ecuador.

INDEX

RESUMEN	4
ABSTRACT	5
LIST OF FIGURES	8
ABBREVIATIONS	9
Chapter 1: Introduction.....	12
1.1 Summary of the Macuchi Formation	12
1.2 <i>Historical background of VMS deposits of Macuchi Formation</i>	13
1.3 <i>Objectives of the review</i>	13
<i>General Objectives</i>	14
<i>Specific Objectives</i>	14
Chapter 2: <i>Geological Evolution of Ecuador</i>	15
2.1 <i>Precambrian</i>	15
2.2 <i>Paleozoic</i>	17
2.2.1. Permian	17
2.3 <i>Mesozoic</i>	17
2.3.1 <i>Triassic</i>	17
2.3.2 Jurassic	18
2.3.3 Cretaceous.....	19
2.4 <i>Cenozoic</i>	21
2.4.1 Early Tertiary-Eocene	21
2.4.2 Late Tertiary-Miocene	22
Chapter 3: Orogenic Belts	23
3.1 <i>Geodynamics and orogeny of South America</i>	23
3.2 <i>Orogeny formation in Ecuador</i>	23
3.3 <i>Western cordillera</i>	25
CHAPTER 4: Introduction to VMS deposits	29
4.1 Types of VMS deposits	31
4.2 <i>VMS deposits from Subduction Zones</i>	33
Chapter 5: Au-VMS Deposits.....	35
5.1. Transport of Gold Systems (specific mechanisms of Gold transport + variables)	35

5.2 Transport of Gold in mineralization systems	39
5.2.1 Chemical Affinity of Au	39
5.2.2 Solubility and volatility of gold	40
5.2.3 Vapor-liquid transport of gold.....	42
5.3 Occurrence of Gold in minerals.....	43
5.3.1 Gold precipitation processes.....	43
5.3.2 Gold in sulfide minerals.....	45
Chapter 6: Macuchi VMS deposits	47
6.1. Macuchi Formation	48
6.2 El Domo Deposit.....	49
6.3 La Plata Deposit.....	53
6.4 Macuchi Deposit.....	55
Chapter 7: Conclusions and recommendations	56
7.1 Conclusions.....	56
7.2 Recommendations	59
References	60

LIST OF FIGURES

Figure 1. Macuchi Formation and Au-VMS deposits location	122
Figure 2. Amazonian Craton Provinces and Colombian Grenville belt.....	16
Figure 3. Intracontinental rift and shear marking the onset of the separation between Central and South American plates.....	18
Figure 4. Jurassic Double subduction zone. Interoceanic island arc of Alao.....	19
Figure 5. The Chaucha/Tahuin terranes are accreted onto the Alao terrane, separated by the Peltetec ophiolite.....	20
Figure 6. Interoceanic island arcs and accretion onto the Chaucha/Tahuin terranes.....	20
Figure 7. Main terranes and faults of Ecuador.	24
Figure 8. Idealized massive sulfide lens illustrating zonation features for hypogene ore minerals. [Ba, barite; Cpy, chalcopyrite; Gn, galena; Po, pyrrhotite; Py, pyrite; Sp, sphalerite].	30
Figure 9. A schematic composite section through a VMS alteration system in the Bathurst mining camp as an example of a VMS proximal alteration zone metamorphosed to greenschist-grade mineral assemblages.	31
Figure 10. The formation of mature arc and ocean-continent subduction fronts resulted in successor arc and continental volcanic arc assemblages that host most of the felsic-dominated and bimodal siliciclastic deposits.....	33
Figure 11. Bivariate plot of gold grade versus tonnage for VMS deposits.	366
Figure 12. Schematic illustration of the various types of gold deposits shown at their inferred crustal levels of formation.....	37
Figure 13. Concentration ratios for sulphur, gold, and associated metals measured in coexisting vapor and hypersaline liquid inclusions from boiling assemblages in quartz from porphyry Cu–Au–Mo and related deposits.....	44
Figure 14. Grade vs. Resources of Macuchi VMS deposits	47
Figure 15. Stratigraphy of the El Domo area, including the massive sulfide zone.....	50
Figure 16. Au and Ag concentrations in El Domo VMS deposit.....	53
Figure 17. Lithostratigraphic sequence of the La Plata.....	54
Figure 18. Paragenetic mineral sequence at the La Plata deposit.	55

ABBREVIATIONS

Ag	Silver
As	Arsenic
Aspy	Arsenopyrite
Au	Gold
$\text{Au}(\text{HS})^{2-}$	Disulfurized gold complex
$\text{Au}(\text{OH})$	Gold hydroxide
$\text{Au}^{+1}, \text{Au}^{+3}$	Gold cations
Au_2Cl_2	Gold trichloride
AuCl^{4-}	Chloroauric acid
Ba	Barite
BGS	British Geological Survey
Bo	Bornite
Br_2	Molecular bromine
Cl	Chlorine
Cl^-	Chlorine ion
CN_2	Cyanogen
CODIGEM	Corporación de desarrollo minero metalúrgico
Cpy	Chalcopyrite
Cu	Copper
$\text{Cu}_{12}\text{As}_4\text{S}_{13}$	Tenantite
$\text{Cu}_6\text{Fe}_2\text{SnS}_8$	Mansonite
Fe^{+3}	Iron cation
FeS	Iron sulfide
Fm	Formation
Gn	Galena
HFSE	High field strength elements
HS^-	Bisulphide anion
HS_2	Hydrogen sulfide

IAV	Interandian valley
K	Potassium
Km	Kilometer
LREE	Light rare earth elements
Ma	Millions of years
Mn ⁺⁴	Manganese cation
MORB	Mid ocean ridge basalt
MVT	Mississippi valley type
OIB	Ocean island basalt
P	Pressure
Pb	Lead
Po	Pyrrhotine
PRODEMINCA	Proyecto de desarrollo minero y control ambiental
Py	Pyrite
Qtz	Quartz
S	Sulfur
S ₂ O ₃ ²⁻	Thiosulfate anion
Se	Selenium
SEDEX	Sedimentary exhalative deposits
Sp	Sphalerite
Sr	Strontium
T	Temperature
Te	Tellurium
U	Uranium
VHMS	Volcanogenic hosted massive sulfide
VLF	Very low frequency
VMS	Volcanogenic massive sulfide
VMS	Volcanogenic massive sulfide
Zn	Zinc

Zr	Zirconium
----	-----------

Chapter 1: Introduction

1.1 Summary of the Macuchi Formation

The Macuchi Formation is an island arc made up of a single lithostratigraphic unit covered by sequences of sediments after its emplacement onto the continent (collision). It is located on the edge of the Western Cordillera (between $2^{\circ} 30' S$ and the Equator line), limited by the Pallatanga Block and the regional N-S Chimbo-Toachi fault (Hughes and Bermúdez, 1997; Hughes and Pilatasig, 2002). It is located in the Western mountain range, ~100 km southwest of Quito. The Macuchi arc hosts three recognized VMS deposits including La Plata, El Domo, and Macuchi (Fig. 1). The formation of these deposits is interpreted by the compression tectonic regime on the Macuchi island arc, which was accreted to the continental margin during the Paleocene-Eocene age (Cuenca, 2018), forming pull-apart basins within a regional transpressive setting.

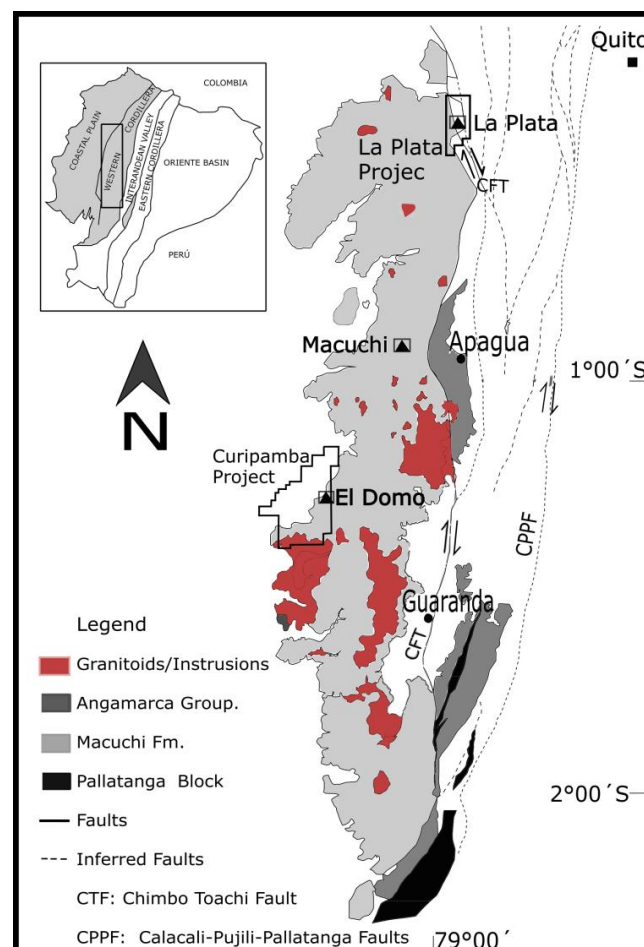


Figure 1. *Macuchi Formation and Au-VMS deposits location.* (Modified from: Vallejo et al., 2016)

1.2 Historical background of VMS deposits of Macuchi Formation

The mining activity in the Macuchi Formation dates back to the Spanish colonial era in 1750. The mine reserves of Macuchi were calculated at 650,000 tons and 472,156 tons were exploited since 1750. In the period of 1940-1945, 24,000 tons of ore were exploited, having 5% Cu, 11.6 g / t Au and 68 g / t Ag. In 1960, the Central University of Ecuador (UCE) began a mineral exploration campaign with the support of foreign researchers. UCE (in 1981) took over the mining district and negotiated with Ecuatomin S.A. conducting cartographic and geological studies in the area, geochemical sampling of various types, geophysical studies (electromagnetics, magnetics, and VLF). The production of a geological map was a decisive step in the exploration and prospection of the Macuchi Formation by the British Geological Survey (BGS) and the Research & Geological Mining Metallurgical Development Corporation (CODIGEM; 1997). This map defines a volcanoclastic sequence (around 80%), with interbedded lavas or sub volcanic sills over the Macuchi Formation and establish that it belongs to submarine effusive eruption activity (Cuenca, 2018).

In 2000, the Mining Development and Environmental Control Project (PROENDEMICA) reported massive volcanogenic sulfide (VMS) occurrence in the Real (Alao-Paute districts; Alao Unit) and Occidental (La Plata district; Macuchi Formation) mountain ranges during the evaluation of mining districts in Ecuador. The formation of these VMS deposits is associated with oceanic island arcs during the Paleocene-Eocene (e.g. Macuchi) and during the Jurassic-Cretaceous (e.g. Alao) (Cuenca, 2018).

The lithostratigraphy of “El Domo” deposit was the next step in the coming years. The geological map of the project "Las Naves" focused on the analysis of structural features and the characterization of intrusive bodies and breccias of the unit (e.g. Pratt et al., 2008). The sulfides deposition from “El Domo” deposit occurred during a tectonic event through active faults and the formation of graben after the formation of Macuchi Formation (Cuenca, 2018).

1.3 Objectives of the review

The current review will create a base knowledge of the Au-rich VMS mineralization system of the Macuchi Formation, Ecuador. It focuses on understanding the regional tectonics and their formation processes. This compilation will be helpful for future academic studies and industrial purposes. The main objectives include:

General Objectives

- Interpretation of the formation processes of these deposits.
- The characterization of the Ecuadorian VMS deposits.
- The creation of a base knowledge comparable to similar deposits in the Andes and worldwide.

Specific Objectives

- Determination of the physico-chemical factors that control the occurrence of gold in these deposits.
- Generation genetic model/s for the formation of the Macuchi Au-rich VMS deposits.

Chapter 2: Geological Evolution of Ecuador

2.1 Precambrian

The agglutination of continental blocks that formed the Rodinia Supercontinent (~1000 Ma) produced the Grenville belts. The collisional state (between 1300-1000 Ma) suffered by the continental blocks created the Grenville Collisional Orogeny, characterized by belts formation and metamorphism (Cordani et al., 2010). The collision between Laurentia and Amazonia created the Grenville and Sunsás belts. The collision of both belts was the paleo-north part of the Amazonia continental block, which through tectonics turned and forms the southwestern margin of the Amazon craton (See Fig 2). Rock analysis has recognized the presence of the Sunsás belt in Bolivia and southeast Perú, which could be extended through the oriental part of Ecuador (Chew et al., 2011; Spikings, 2019; JTorro Álava, 2019, personal comm.). Furthermore, there is evidence that Grenville orogeny extends until Colombia. The Grenville event in Colombia is related to the welding of Precambrian allochthon Chicamocha terrane to the Guyana shield and a subsequent rift-drift phase that enhanced the formation of Late Paleozoic- Cambrian basins (Cediel, 2019). The presence of Sunsás Belt at Eastern Perú and the Grenville event in Colombia suggests that Ecuador can have Grenville orogeny as well (Sunsás at Oriente and Grenville at Northern Ecuador; See Fig.3).

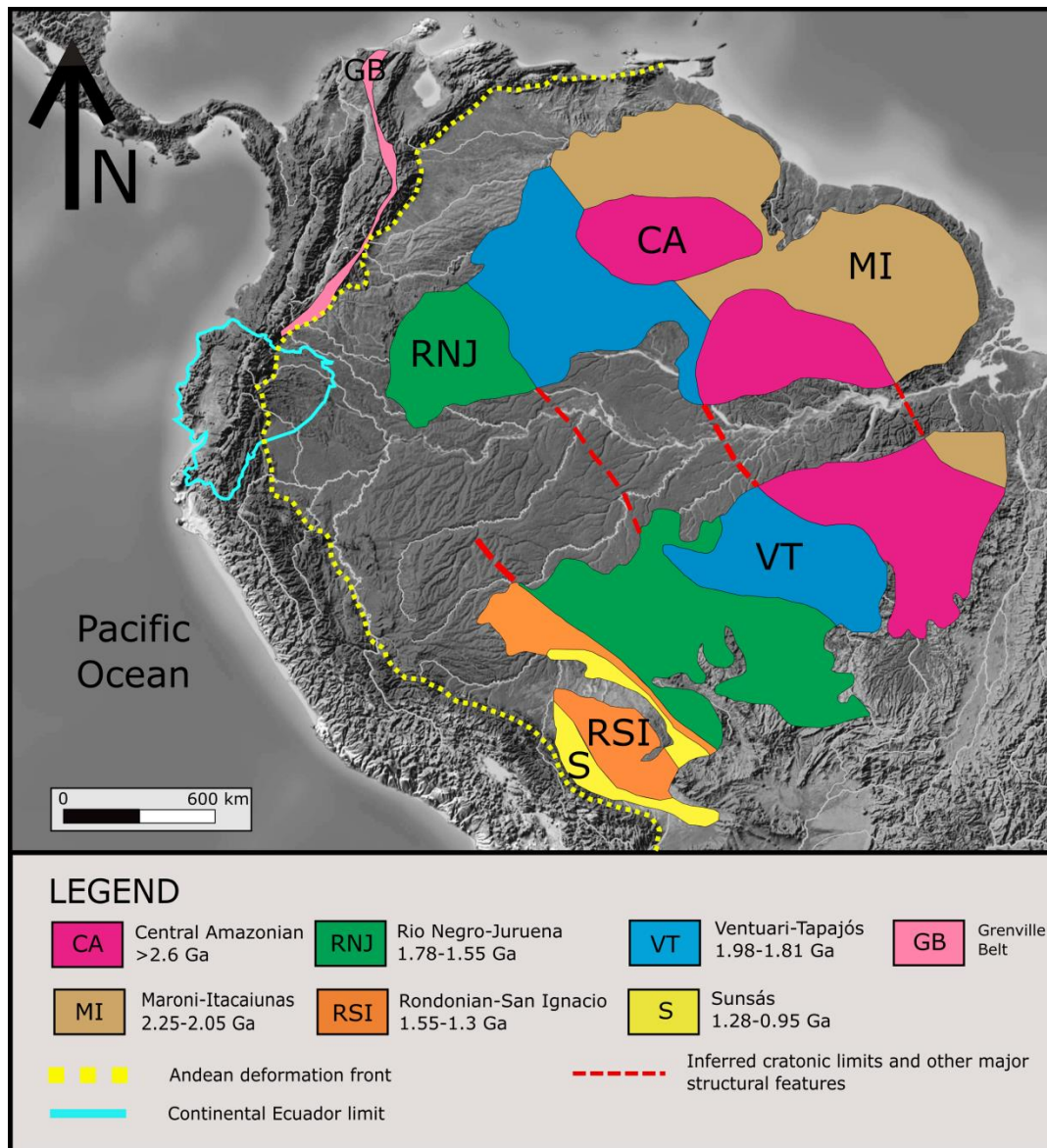


Figure 2. Amazonian Craton Provinces and Colombian Grenville belt. (From: Cediel, 2019; and Chew et al., 2011)

The shield (Tapi granulite) form the metamorphic amazonian region substratum, extended below the Oriente basin. It is composed by micaceous gneiss in NE of the Oriente basin, mica schist at the west and granulites at the Tapi oil wells in Putumayo (Medium-dark gray granoblastic crystalline gneissic granulites of $1.6 \pm 0,048$ Ga (Rb-Sr) (Vera, 2016; Teixeira et al., 1989).

The xenocryst zircons analysis supports the idea that the Guyana shield remains below the Andes. Zircon analysis at Marcabeli Pluton(“El Oro” province) inhered Zr ages of 540 Ma, 2.22 and 2,876 Ga; the Tres Lagunas granitoids (southern Cordillera Real) shows Zr ages of 2.9-2.85 Ma. Also, Nd-depleted Mantle models (TDM) gives 1.6-1.4

Ga ages for Tres Lagunas and Marcabelli granitoids (Noble et al, 1997). The similarity of these ages with the gneissic granulites at Putumayo suggests the Guyana Shield were partially melted during the magma ascension in the Eastern Cordillera.

The Precambrian metamorphic belt goes through the Cordillera Real. For example, the Amotape-Tahuin ranges located in southern Ecuador (that continues to the south to form the Olmos Massif in Perú) and a wider metamorphic belt in Northern Ecuador (next to the Esmeraldas fault; Vera, 2016). In addition, Central Colombian Cordillera radiometric analysis dated 1,6Ga; > 1,2Ga (granulites) & 850Ma (pegmatite dikes) at Garzón Massif, enhancing the idea of the presence of the Precambrian rocks in Northern Ecuador.

2.2 Paleozoic

2.2.1. Permian

The analysis of scattered rocks in the mountain ranges of Ecuador and Colombia support a continental arc environment during the Permian (288-253 Ma) which extended from North America to southern Peru. The northwestern margins of South America evidence the formation of Pangea during the Permian, as well as its subsequent fragmentation during the Triassic. The subsequent fragmentation of the continental arc (due to subduction of the Caribbean plate) in northern South America during the Cenozoic removed and moved blocks eastern side (Chiaradia et al., 2004). The continuous compression triggered regional metamorphism characterized by the amalgamation and thickening of western Pangea 250 Ma ago. Later, the fragmentation of Pangea (209 Ma) triggered the opening of the Proto-Caribbean Ocean and the beginning of the formation of the Andes (Vallejo et al., 2019).

2.3 Mesozoic

2.3.1 Triassic

The formation of a Triassic rift marks the beginning of the separation of Pangea at 240 Ma. The early separation of Pangea (rift) and the attenuation of its western edge show signs of a process of separation of the continents (Chiaradia et al., 2004a). The weakening of the crust, due to an extensive regime, allowed the ascent of the Mantle,

promoting the formation of igneous provinces and promoting the separation of Pangea. In northern South America (Ecuador-Colombia), the extension process in the retro arc promoted the transition from rift-drift to the deflection of Huancabamba (Peru) at 223Ma, creating the lithosphere of the proto-Caribbean ocean (Vallejo et al., 2019).

TRIASSIC

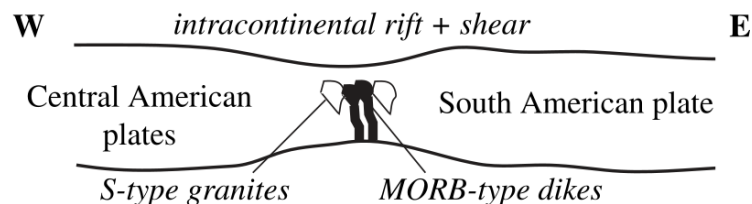


Figure 3. *Intracontinental rift and shear marking the onset of the separation between Central and South American plates.* (From: Chiaradia et al., 2004a).

2.3.2 Jurassic

The extensional rift process began in southeastern North America at 230 Ma (Withjack et al., 2002). The separation of the continental crust led to the formation of Central Atlantic Magmatic Province (through a giant dyke swarm injection) at 200 Ma (Beutel, 2009) and the formation of an oceanic crust beneath North and South America at 180 Ma (Vallejo et al., 2019). These events favored the attenuation of the margins and the elevation of the mantle, initiating the separation of Pangea. The Pangea rupture used already weakened suture zones (e.g., the South America – Yucatán – North America – Central African Sutures) which concentrated mantle melts, forming igneous provinces and a subsequent ocean formation (Buitter & Torsvik, 2014; Vallejo et al., 2019).

The Triassic-Jurassic continental arc formed at 209 Ma in the Santander Massif and extended westward to the Cordillera Real at 189 Ma (Spikings et al., 2015; Vallejo et al., 2019; van der Lelij et al., 2016). This Jurassic extension produced several effects on the region such as:

- **(202-201 Ma)** The extrusion of the Central Atlantic Magmatic Province (Davies et al., 2017).
- **(195 Ma)** The separation of North America, Yucatán, and South America formed the Proto-Caribbean Sea and Atlantic Ocean (Beutel, 2009; Pindell & Kennan, 2009; Vallejo et al., 2019).

- (189-145 Ma) Eastward Jurassic arc migration (trench direction) (Cochrane et al., 2014; Spikings et al., 2015; Vallejo et al.2019).
- Grabben formation (Vallejo et al., 2019; Bartok, 1993).
- Deposition of sedimentary sequences and unit formations (Jaillard et al., 1990; Toussaint & Restrepo, 1994).

2.3.3 Cretaceous

The double subduction of the proto-Caribbean sea drove (See Figs. 4, 5) the geodynamical evolution during Jurassic-Early Cretaceous. The subduction increased the volcanic activity forming the Alao island-arc terrane, Salado Basin, and several plutons (Azafrán, Abitagüa, and Zamora). The contemporaneous accretion of Tahuin/Chaucha terranes onto Alao terrane during the Cretaceous produced the Peltetec event (Fig.5), characterized by the metamorphism of the Alao (basalt-andesite) and Salado (volcano-sedimentary andesitic rocks) terranes. In addition, the accretion of these terranes produced a western displacement of the subduction margin during the Cretaceous (Chiaradia, 2004a).

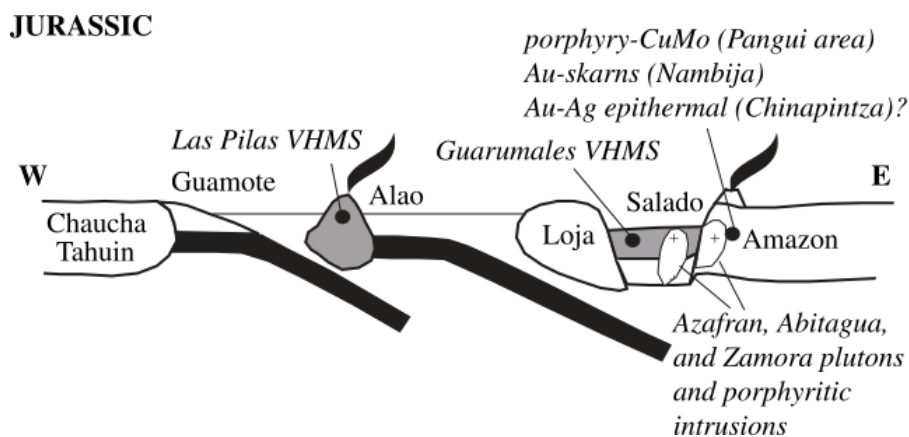


Figure 4. Jurassic Double subduction zone. Interoceanic island arc of Alao (Taken from: Chiaradia et al., 2004a).

LATE JURASSIC-EARLY CRETACEOUS

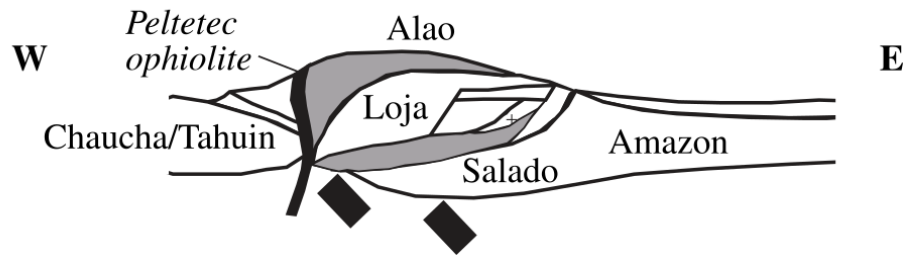


Figure 5. The Chaucha/Tahuin terranes accreted onto the Alao terrane, separated by the Peltetec ophiolite (From: Chiaradia et al., 2004a).

The accretion of several oceanic plateau segments (basalts and gabbros mainly) and the overlying island arc (basalts and andesites) in Northern Ecuador formed the Piñon/Pallatanga and San Lorenzo/Macuchi Formations (Fig. 6), respectively (Chiaradia, et al 2004a). The lateral accretion of Upper Cretaceous oceanic rocks forms the basement of the Western Cordillera and the forearc (Piñon-Pallatanga; Vallejo et al., 2009, 2019). This accretion of ultramafic and mafic rocks into the continental crust was produced in an oceanic hot-spot setting (99-87 Ma) and presents a compositional equivalent to the oceanic Caribbean Plate (Sinton et al., 1998; Van Der Lelij et al., 2010; Kerr 1997; Vallejo et al., 2006, 2019; Villagómez et al., 2011).

LATE CRETACEOUS-EOCENE

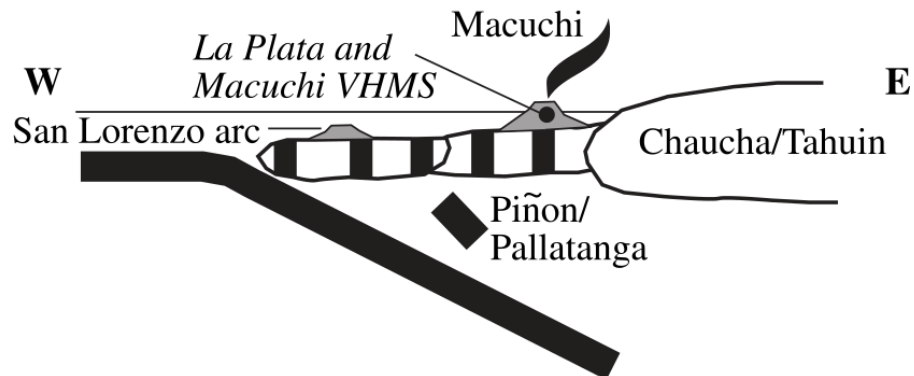


Figure 6 . Interoceanic island arcs and accretion onto the Chaucha/Tahuin terranes. (Taken from: Chiaradia et al., 2004a).

During Late Jurassic-Early Cretaceous, several continental fragments, produced by the separation of the Central and South American plates, accreted to the continental margin of Ecuador. Loja (Paleozoic schist, gneiss Triassic granites and anatexites), Tahuin, and Chaucha (both with similar lithology than Loja Unit) terranes were formed by the

accretion of detached continental fragments onto the Amazon Craton (Chiaradia, 2004b). Furthermore, the oceanic accretion into the continental crust produced metamorphism events and skarn deposit formation. The Southern Cordillera Real (eastern Cordillera) hosts the Nambija Au deposit dated from molybdenite Re-Os ages at 145.92 ± 0.46 Ma (Vallance et al., 2003; Chiaradia, 2004).

2. 4 Cenozoic

2. 4. 1 Early Tertiary-Eocene

The dextral rotation of the Farallón-Nazca plate created an oblique subsidence in the northern Andes during the Eocene. The change in the direction of a tectonic plate is produced by the vector summation of the total movement of the plates, creating a change in the Farrallon-Nazca subduction angle under western South America (Chen et al., 2019; Vallejo et al., 2016). Despite being a compressive regime, the oblique convergence of the plates created a dextral-transpressional regime that formed NE-SW transcrustal faults and a pull-apart-basin (Vallejo et al., 2016). The local extension formed extensional basins (NNE) that, together with the faults, favored the rise of magmas and hydrothermal fluids (Vallejo et al., 2016). The mineralization of the Macuchi VMS systems is located in this environment ≈ 42 Ma ago. The Pallatanga and Chimbo-Toachi faults were created by fragments accreted to the continental limit (Hughes and Pilatasig, 2002) and delimited the extensional zone where the Macuchi mineralization was formed (Vallejo et al., 2016).

The Macuchi Arc activity increased during the Early Tertiary. The Macuchi Formation consists of two main sequences (geochemical and stratigraphically differentiated) defined as Basal Macuchi and Main Macuchi. Basal Macuchi (lower sequence) has mainly a basaltic (E-Pacific MORB) composition while Main Macuchi (upper sequence) has anintermediate composition (basalt-andesite) (Chiaradia, 2004a). Generally, Au-Cu-Zn VMS deposits (La Plata, Macuchi, and El Domo are related to the early Tertiary magmatism (Macuchi island-arc) while porphyries and epithermal deposits are associated with the middle-late Tertiary magmatism (Charadia, 2004a). El Domo deposit shows formational age values of 42.13 ± 0.4 Ma and 41.99 ± 0.37 Ma (Vallejo et al., 2016).

2. 4. 2 Late Tertiary-Miocene

The subduction of the Farallon/Nazca plate, the consequent magmatism, and the accretion of oceanic volcanic arcs produced the western metallogenic belt in Ecuador (Schütte et al., 2012). The Pliocene-Quaternary tectonism enhanced the Andean Uplift (Frutos, 1982), forming the western cordillera and the related Metallogenic belt. The Miocene metallogenic belt deposits follow a Spatio-temporal distribution of arc magmatism produced by the subducting slab geometry and upper plate structures (Sillitoe 1972; Kay et al. 1999; Richards 2003; Schutte et al., 2012). The Late Miocene collision and subsequent subduction of the Carnegie ridge with the northern Ecuadorian margin could be a formational factor of Au-rich deposit formation like Junín, El Corazón in Northern Western Cordillera of Ecuador.

Chapter 3: Orogenic Belts

3.1 Geodynamics and orogeny of South America

The cyclical tectonic activity through the western margin of South America caused the Andean Ridge formation. South America geodynamics related the two tectonic cycles Hercynian and Andean that developed the orogenic structures in the Andean countries during Cambrian-Early Triassic and Late Triassic-Present (Hercynian-Andean, respectively; Frutos, 1982).

The abundance of Precambrian zircons in Paleozoic sediments in South America suggests a tectonic cycle of rapid exhumation during the Devonian-Carboniferous (430-300 Ma). The formation of the Cordillera Real in Ecuador produced the reworking and deposition of these sediments in Amazonian basins of the Cretaceous (Martin-Gombojav & Winkler, 2008). The time of exhumation of these sediments is correlated with the Hercynian/Alleganian orogeny, which deformed the Gondwana supercontinent west margin from 360 to 265 Ma (Ramos and Alemán, 2000; Gambojav et al., 2008).

3.2 Orogeny formation in Ecuador

The subduction of the Farallon / Nazca plate produces distinctive geological structures such as the Andean mountain ranges and the separation of the different physiographic regions of Ecuador. The deformation of the terrain as a result of the compressive-extensive regime created the formation of the Andean Cordillera together with large faulting systems that delimit the physiological regions (Pardo-Trujillo et al., 2020). The physiographic regions of the continental Ecuador are Oriente, Cordillera Real, the Inter-Andean valley (IAV), Western mountain range, and Coastal Zone (See Fig.7). The Ecuadorian regions have formed by collisional-accretional events that deformed the Continental crust. These regions had been formed during the Jurassic-Eocene period through the subduction of Nazca-Pacific Plates under South America, the consequent uplift of the Andean ridges, and several accretion events at western Ecuador (Chiaradia et al., 2004b).

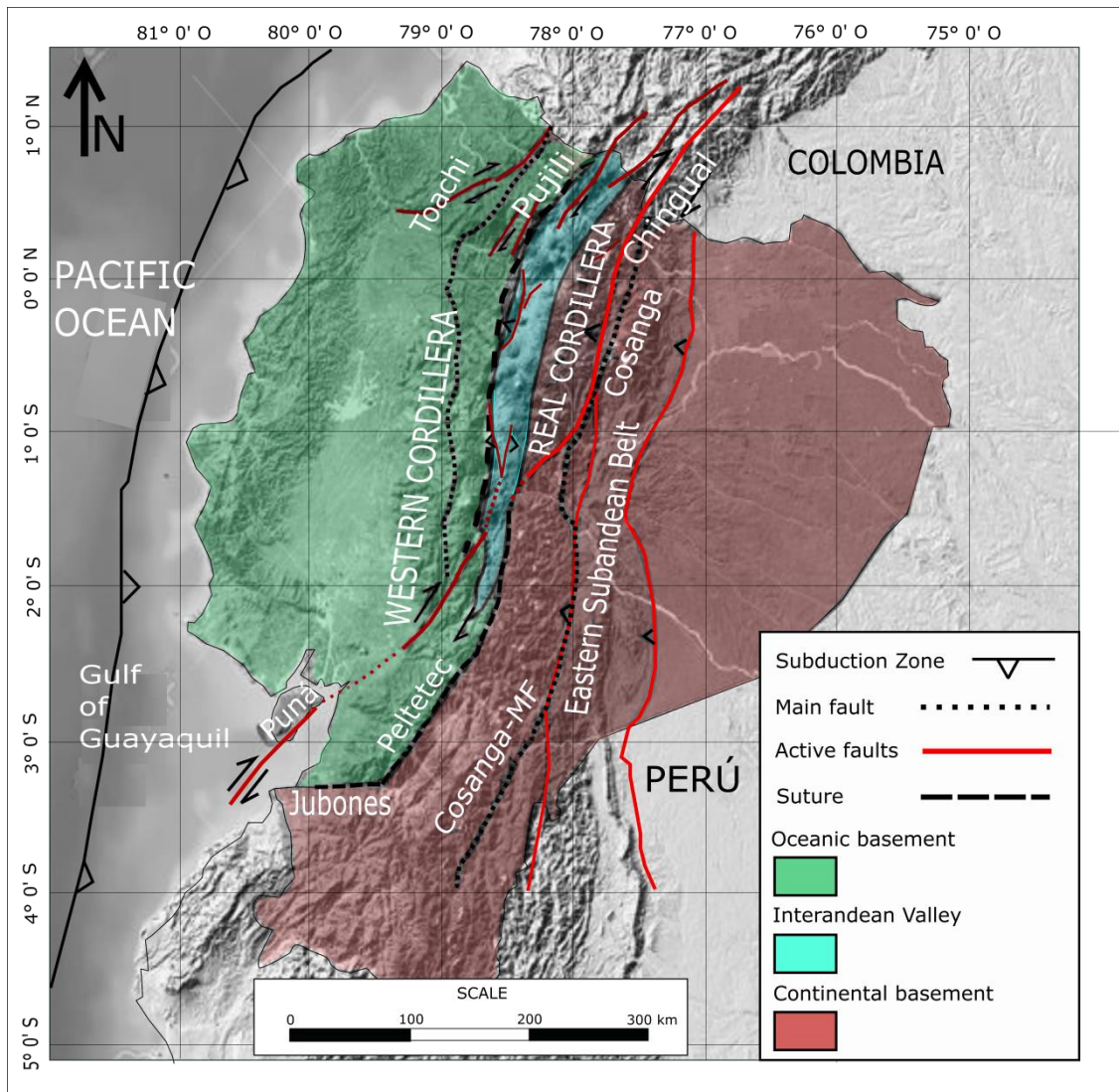


Figure 7. Main terrains and faults of Ecuador (Modified from: Vallejo et al., 2020)

Extensive processes to the east of South America during the Jurassic allowed the formation of the Cordillera Real in Ecuador. The extensive regime extended from Colombia to the north of Argentina and produced the Central Magmatic Province of Atlántico 202-201Ma (Davies et al., 2017). Also, the southwesterly migration of the continental Triassic-Jurassic Arc formed in the Santander massif 209 Ma ago and the formation of the Cordillera Real in Ecuador 189 Ma ago (composed by Paleozoic to Jurassic metamorphic rocks and Mesozoic granitoids) (Vallejo et al., 2019, 2020; Cochrane et al., 2014a; Spikings et al., 2015)

Cordillera Real in Ecuador formed at the same time of formation of a grab. The Cordillera Real includes different sequences and units (Vallejo et al., 2019; Bartok,

1993; Toussaint & Restrepo, 1994; Jaillard et al., 1990) on the pre IAV until its delimitation with the formation of the Western Cordillera during the Eocene-Miocene. The IAV covers metamorphic rocks (tectonic melange; Pujili Unit) at the boundary between the collision of continental and oceanic blocks that formed the Western mountain range, originating the Pallatanga-Pujili-Calacalí fault (Spikings et al., 2005). The IAV was formed by strike-slip processes and is limited by Pujili-Pallatanga-Calacalí Mega shear fault to the West (between Western Cordillera and IAV) and the Peltetec Fault to the East (between the Cordillera Real and IAV; Spikings et al., 2005).

The Western mountain range is composed of mafic and intermediate rocks covered by sedimentary and volcano-sedimentary units (from the Late Cretaceous to the Miocene). These sedimentary units are produced by the activity of faults arranged in a north-south direction, covering the allochthonous basement (Pardo-Trujillo et al., 2020). The western mountain range is limited to the east by the Calacali-Pujili-Pallatanga fault and to the west by the coastal plain, being divided in the center by the Chimbo-Toachi fault (crossing the Macuchi Formation; See Fig. 2).

The creation of the Western Cordillera occurred by the compressive regime and the accretion of oceanic blocks in western Ecuador since the Late Cretaceous (Pardo-Trujillo et al., 2020). The compressive tectonic regime and positive buoyancy of the oceanic plates produce the collision, and the consequent accretion of them into the continental margin (Pardo-Trujillo et al., 2020). The first period of oceanic collision-accretion was produced by the subduction of the Pallatanga terrain below the Western continental margin between 80 and 60 Ma ago (Spikings et al., 2005). The second accretion period involves a dextral collision between the Macuchi and Pallatanga terrains, forming the Chimbo-Toachi fault 40 Ma ago (Spikings et al., 2005; Spikings et al., 2001).

3.3 Western cordillera

The Western Andean mountain range is a mountain chain created by a compressive regime and the accretion of oceanic blocks on the western continental margin of Ecuador (Vallejo et al., 2020). The Western mountain range consists of intrusive and extrusive rocks of mafic-intermediate composition that were increased to South

America during the late Cretaceous period covered by sedimentary and volcano-sedimentary units of complex distribution (Pardo-Trujillo et al., 2020). The allochthonous basement of the Western mountain range is the Pallatanga formation and it divides in:

- 1) The basement made up of basalts of the Pallatanga formation and ultramafic rocks of San Juan.
- 2) Submarine basaltic lavas from the late Cretaceous and rocks of the Arch "Rio Cala".
- 3) Volcanic and subvolcanic rocks from the Tandapi Unit (Maastrichtian to Paleocene).
- 4) Submarine deposits of the Angamarca Group (Paleocene-Eocene).
- 5) Calco-alkaline volcanic rocks from the Oligocene-Miocene (including the San Juan de Lachas and Saraguro formations; Pardo-Trujillo et al., 2020).

The E-MORB basalts from the Pallatanga formation show similar chemical composition patterns to the basalt from the Caribbean plate, suggesting that its formation occurred in an intraoceanic location (Luzieux et al., 2006; Kerr et al., 1997; Pardo-Trujillo et al., 2020). Zircon analysis of gabbros from the San Juan Formation determined U-Pb 87.1+1.7 Ma as the age of crystallization of this oceanic plate (Vallejo et al., 2009; Pardo-Trujillo et al., 2020). In addition, the oceanic plates show a thickness of 10-30 km, giving them positive buoyancy and incorporating them to the continental margin instead of being subducted (Sinton et al., 1998; Pardo-Trujillo et al., 2020).

The Yunguilla formation was deposited in a fore-arc basin distributed along the continental margin of South America (Vallejo et al., 2019,2020), overlapping the Pallatanga formation (Hughes and Pilatasig, 2002). The Yunguilla formation consists of fine sequences of massive siltstones and Qtz-rich fine-grained sands, with turbiditic sequences; probably intermediate to distal Submarine fan (Hughes et al., 1997) alternated with mudstones (Pardo-Trujillo et al., 2020). The fossil record (Phylloceras sp., Exiteloceras sp., and ammonites) relates it to the Late Campanian and Early Maastrichtian ages (Jaillard et al., 2004). Also, the mineral composition (Zirconium, granite, epidote, tourmaline, rutile, and minor titanite, anatase, brookite) shows a

considerable amount of granitic and metamorphic debris from the rework of ancient formations of the Cordillera Real (Vallejo et al., 2019).

The Tandapi Unit consists of sequences of volcanic rocks (porphyritic andesites with plagioclase, hornblende, and pyroxene), tuffs, and conglomerates (andesites and breccias; Pardo-Trujillo et al., 2020). The Tandapi Unit covers Pilatón Formation, dated from Paleocene to Eocene ages (Egüez and Bourgois, 1986). However, the dating of groundmass ($^{40}\text{Ar} / ^{39}\text{Ar}$ 58.1 + 1.95 Ma; 61 + 1.09 Ma; Vallejo et al., 2009) and plagioclase ($^{40}\text{Ar} / ^{39}\text{Ar}$ 63.96 + 10.7 Ma; Vallejo et al., 2009) suggests a period of clast deposition between the late Maastrichtian and the Early Paleocene (Pardo-Trujillo et al., 2020).

The Angamarca group is composed of sequences of siliciclastic sedimentary rocks (turbiditic sandstones, conglomerates, and limestones) deposited between the Paleocene to the Oligocene (Hughes et al., 1997) and is subdivided between the formations (base to top) Pilalo, Saquisilí, Apagua, Unacota and Rumi Cruz (Hughes et al., 1997; Vallejo, 2007).

The Pilalo formation is composed of coarse-grained turbiditic sands, black shales, siltstones, reworked tuffs, and matrix-supported breccias (Egüez, 1986). The fossil content (Rzehakina Epigon foraminifera) obtained near the Alambí River (near to Nono-Tandayapa road) suggests its formation during the Paleocene (Savoyat et al., 1970).

The Saquisilí formation is made up of dark gray micaceous sandstone, siltstones, and partial calcareous strata (Vallejo et al., 2020). The microfossil analysis dates the Saquisilí formation in the early to middle Paleocene (Hughes et al., 1997).

The Apagua formation is made of medium-grain sandstones (composed mainly of Qtz, Mafic minerals, lithics, and feldspars), siltstones, and turbiditic bed shales (Vallejo et al., 2007; 2019; 2020). The fossil ages range from Middle Paleocene to Middle Eocene (Hughes et al., 1997). The Rumi Cruz Unit (youngest unit of the Angamarca group) is composed of quartz-rich sandstones with Cross stratification, red mudstones, and conglomerates (probably from fan delta systems; Hughes et al., 1997; Vallejo et al., 2020).

The San Juan de Lachas formation presents matrix-supported breccias with intercalations of andesitic lavas and volcanic deposits (Vallejo et al., 2020). The analysis of the andesitic lavas shows a calcalkaline composition, with an age K-Ar 32.6Ma (hornblende from andesitic dyke). However different studies have given a wide range of dates, for example K-A dated a hornblende and a plagioclase at 19.8 + 3 Ma & 36.3 + 3Ma, respectively (Boland et al., 2000). Guallabamba river samples gave a Zircon fission-track date of 23.5 + 1.5 & 24.5 + 3.1 Ma (Boland et al., 2000) and $^{40}\text{Ar} / ^{39}\text{Ar}$ analysis of hornblende dated 32.9 + 1.2 Ma (Vallejo, 2007).

CHAPTER 4: Introduction to VMS deposits

Volcanogenic Massive Sulfides (VMS) are exhalative deposits formed on the seafloor and sub-seafloor through discharges of metal-enriched hydrothermal fluids (Eckstrand et al., 1995; Galley et al., 2007). The source of these metals is related to alteration processes of the host rocks, where the convectational circulation of the water (though the ocean floor), changes in temperature and pH enhancing the leaching of metals from the surrounding rock and depositing them into the ocean bottom. The VMS deposits have significant amounts of Zn, Cu, Pb, Ag, and Au, and minor concentration of Co, Sn, Se, Mn, Cd, In, Bi, Te, Ga, and Ge (Galley et al., 2007).

Volcanogenic Massive Sulfides are strata-bound (typically of lensoidal or sheet-like form) bodies of sulfide minerals precipitated in extensional seafloor environments. These polymetallic deposit ranges from Early Archean to Holocene in age and the mineralogy corresponds to abundant Fe sulfides like pyrite (Py) and/or pyrrhotite (Po) together with variable amounts of chalcopyrite (Cpy), sphalerite (Sp), and galena (Gn), bornite (Bo), chalcocite, arsenopyrite (Aspy), and tennantite-tetrahedrite. Many of these deposits overlie sulfide-bearing vein systems called “stringer” or “stockwork” (Fig.8), which are the fluid flow conduits of the deposit (Shanks et al., 2012).

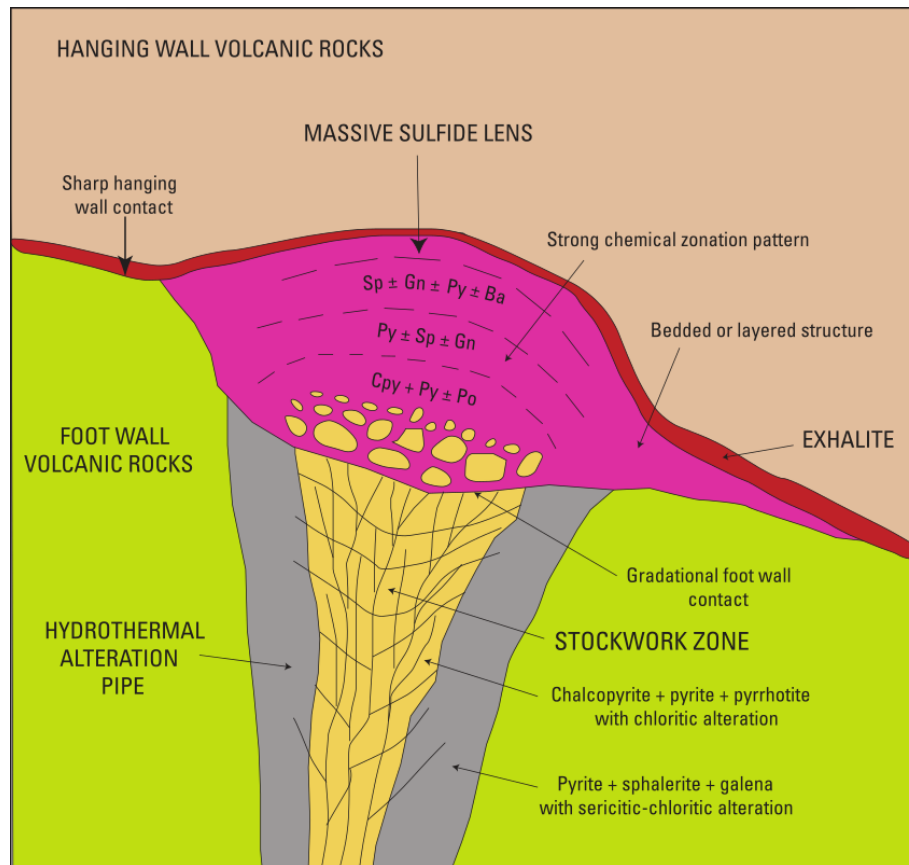


Figure 8. *Idealized massive sulfide lens illustrating zonation features for hypogene ore minerals. [Ba, barite; Cpy, chalcopyrite; Gn, galena; Po, pyrrhotite; Py, pyrite; Sp, sphalerite]* (Taken from: Shanks et al., 2012).

Volcanogenic Massive Sulfide deposits form stratigraphic levels (horizons) which are determined by changes in the composition of the underlying volcanic rocks. The massive sulfide body presents commonly zonations due to the hydrothermal circulation through the footwall, having major amounts of Fe+Cu (Py, Po & Cpy) at the base and Zn+Fe±Pb±Ba (Sp, Gn, Py, Ba) at the top (See Fig 8; Shanks et al., 2012). The passage of hydrothermal fluids creates alteration zones in the footwall of the deposit. The alteration can extend up to several kilometers away from the center of the deposit, creating zones defined by the abundance of specific minerals (See Fig 9). The presence of Fe-chlorite, quartz, sulfide and talc minerals is commonly abundant in the center of the stockwork (zone 1) while it becomes richer in quartz and sulfide concentrations towards the lower contact (zone 2). An extensive zone (zone 3) rich in Fe-Mg-chlorite-sericite covers the two previous zones, presenting phengite in the hanging wall that covers the sulfide lens. The outermost alteration zone (zone 4) is rich in sericite,

phengite, Mg-chlorite, \pm albite, \pm carbonate, and \pm barite, and can occur on the hanging wall (laterally and above the massive sulfide lens; Galley et al., 2007).

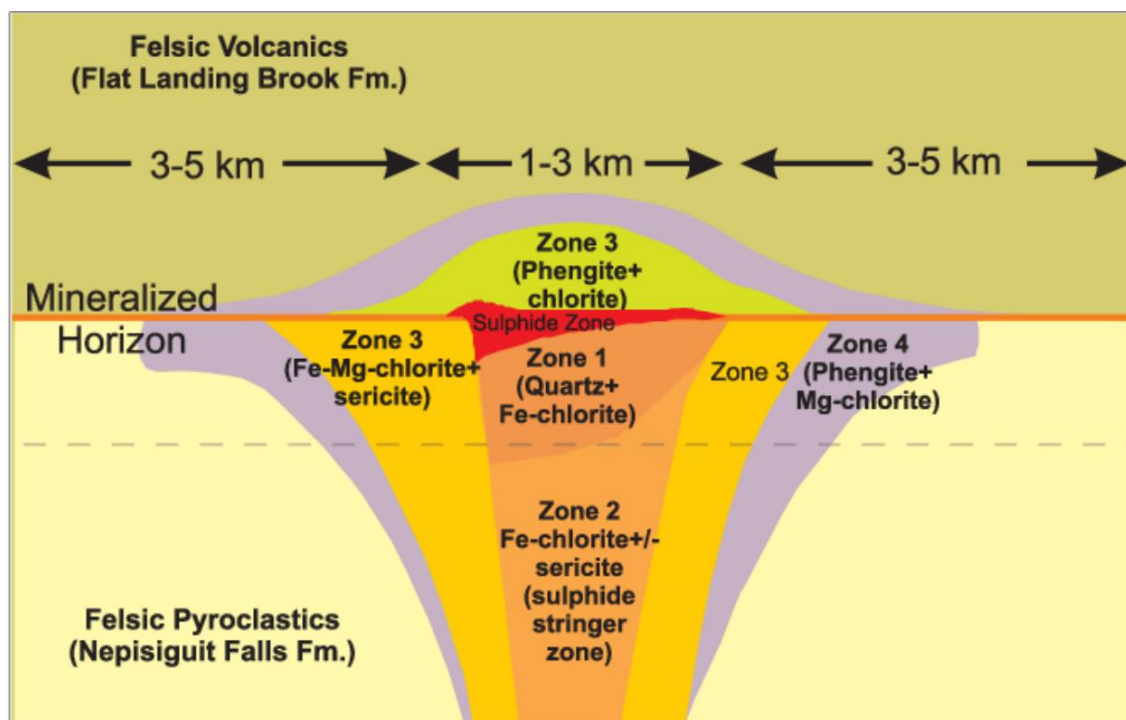


Figure 9. A schematic composite section through a VMS alteration system in the Bathurst mining camp as an example of a VMS proximal alteration zone metamorphosed to greenschist-grade mineral assemblages. (Taken from: Lentz and Goodfellow 1994; Yang et al. 2003)

4.1 Types of VMS deposits

Volcanogenic Massive Sulfide deposits occur in extensive geodynamic environments and form from a syngenetic exhalation of metalliferous hydrothermal fluids on the seabed. In addition, they are associated with specific rocks (mafic and felsic) and with certain petrochemical assemblages (indicative of abnormal temperature formation (Piercey, 2011)). VMS deposits are produced from thermal sources associated with the circulation of marine water within volcanic sequences on the ocean floor.

There are different ways to classify VMS deposits (e.g., metallic content, locality, geodynamic setting) but the most used is the lithostratigraphic classification, which is divided into five groups: (1) mafic (Cyprus type); (2) mafic-siliciclastic (Besshi type); (3) bimodal-mafic (Noranda type); (4) bimodal-felsic (Kuroko-type); and (5) felsic-siliciclastic (Bathurst-type), as followd:

- Cyprus type: Cu (\pm Zn) \pm Au, associated with tholeiitic basalts of ophiolitic assemblages. Typical examples occur on the island of Cyprus in the Mediterranean Sea.
- Besshi type: Cu-Zn \pm Au \pm Ag, associated with sedimentary rocks with a terrigenous contribution, turbidites associated with intraplate basalts (e.g. Oman, Bay of Islands, Slide Mountain. Piercey, 2011)
- Noranda type: Cu-Zn \pm Au \pm Ag, associated with much differentiated volcanic rocks from basalts to rhyolites in marine basins <1 km deep. Currently present in greenstone strips in the Precambrian shields (as in Canada). Their tectonic framework is a matter of debate, but they appear to have formed in subsided basins bounded by faults, possibly in back-arc sections (e.g. Flin Flon, Kidd Creek, Rambler., Piercey et al., 2011).
- Kuroko type deposits are deposits rich in Cu-Zn-Pb + Au + Ag and are associated with bimodal volcanism of tholeiitic lavas and calc-alkaline pyroclasts. They formed mainly in shallow underwater basins in back-arc settings. The geological environment has specific rock types such as rhyolites, dacites, basalts, and associated sediments (organic-rich mudstones & Shales) with flow textures, tuffs, breccias, deposited sediments, and felsic domes (Ishihara, 1974; Franklin et al., 1981; Hutchinson et al., 1982; Ohmoto and Skinner, 1983)(e.g. Buchans, Mount Read, Eskay Creek, Piercey et al., 2011).
- Bathurst Type: It relates to HFSE-enriched rhyolites, MORB/alkalic basalts. The mineralization is located in the transition from felsic-dominated to mafic-dominated magmatism (Piercey, 2011). Caribou Deposit (Bathurst Mining Camp) formed in the Ordovician (470– 465Ma) in a back arc continental rift. It mineralizations presents massive, bedded and brecciated sulfides with stringers (Py & Sph & Gn & Cpy & Mt & Po & Aspy) (Mercier-Langevin et al., 2010).

- Besshi type: (Cu-Zn±Au±Ag) belongs to the mafic-siliciclastic group of VMS. It formed in deep sedimentary basins related to basaltic volcanism. It presents an intercalation of sedimentary rocks with MORB (Ultramafic and basalt/andesite rocks), OIB and boninite (Piercey, 2011).

4.2 VMS deposits from Subduction Zones

Volcanogenic Massive Sulfide deposits formed mainly in oceanic and continental arcs, rifted arcs, and back-arc settings (Franklin et al., 1998; Allen et al., 2002). The back-arc setting deposits are associated with the formation of a mature island arc in an increased oceanic terrain, which is being subducted, in turn forming a continental volcanic arc (Fig 10) (Source: Galley et al., 2007). The thickness of the oceanic plates and the angle in the descent during subduction play an important role in the accretion of oceanic land to the continental margin. In post-accretion environments, the thickening of the crust fragments can generate extensive regimes due to the change of angle in subduction, subduction motion in a session of the plate boundaries, or the change of direction along the convergent plates (Ziegler, 1992; Hamilton, 1995).

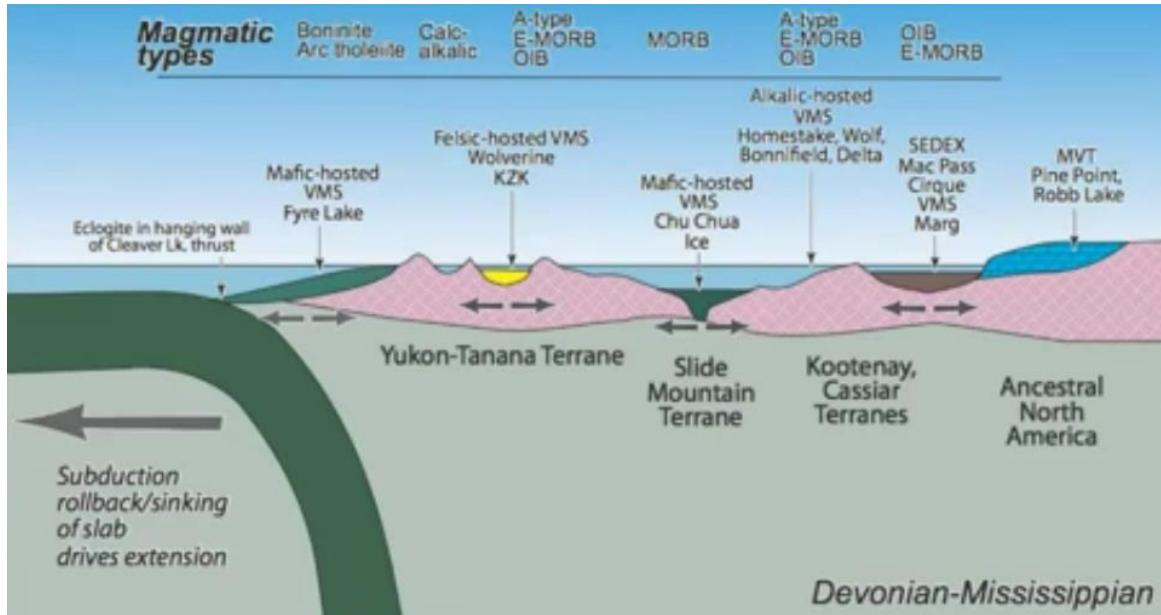


Figure 10. The formation of mature arc and ocean-continent subduction fronts resulted in successor arc and continental volcanic arc assemblages that host most of the felsic-dominated and bimodal siliciclastic deposits. (Taken from: Colpron et al., 2007)

The extensive regime encourages the creation of a strike-slip basin at the location of the oldest arc (Galley et al., 2007). The reduction of the thickness of the oceanic plate will create a depression (basin) that can be filled with bimodal volcanic sediments and enhance the ascendant of magma, creating magmatism associated to porphyry systems (Richards, 2003). These conditions will form different types of mineral deposits, including epithermal and VMS deposits (Galley et al., 2007).

Chapter 5: Au-VMS Deposits

5.1. Transport of Gold Systems (specific mechanisms of Gold transport + variables)

Au-VMS globally represent 1.2% (1453 metric tons) of world gold production and reserves (Dubé et al., 2007). The most representative world class deposits in gold production and reserves are the Horne mine (Canada) with 331t Au, Mt. Morgan (Australia) with 296.31t Au and Bousquet 2-La Ronde 1 (Canada) with 119.55t Au (see Table 1; Dubé et al., 2007). Au-VMS ranges from small sulfide lenses (less than 2 t Au in 2-10 Mt) to giant-sized lenses and stockwork-stringer zones (> 300t Au in > 50 Mt) in size, from 6 Mt of ore to > 85 Mt in tonnage (Dubé et al., 2007). In addition, the world average of these deposits is 7.69 g / t Au, with Canadian Au-VMS being the most representative with an average of 7.83 g / t Au (varying between 1.5 to 38 g / t) (Dubé et al., 2007).

Table 1. Grade and tonnage of world-class Au-VMS deposits with at least 30 tonnes Au in production and reserves (Source: Dubé et al., 2007).

Deposit name	Country	Tonnage (Mt)	Au (g/t)	Ag (g/t)	Cu (%)	Pb (%)	Zn (%)
Bousquet 1	Canada	6.44	5.55				
Agnico Eagle	Canada	6.93	5.18				
Bousquet 2 - LaRonde 1	Canada	23.26	5.14	2.12			
Horne	Canada	54.3	6.10	13.00	2.22		
LaRonde	Canada	43.45	4.23	52.12	0.32		2.72
Penna	Canada	13.92	4.74	19.53	1.21		1.82
Quemont	Canada	2.49	44.38	2087.68			
Eskay Creek	Canada	80.74	3.67	0.74	0.72		
Mt. Morgan	Australia	6.2	10.00				
Hassai	Sudan	8.3	15.09	48.31	1.42		
Boliden	Sweden	4.4	6.47	61.00	2.13		5.35
Abyz	Kazakhstan	11.2	4.20	560.94	0.01	4.07	10.88
Greens Creek	U.S.A.						

The Au content and the base metal ratio are essential in the characterization of Au-VMS. VMS deposits classified depending on their Au content (g / t vs. tonnage ratio) between: Au-VMS (> 3.46 g / t Au), Anomalous-VMS (> 31T Au) and Au-rich VMS (> 3.46 g / t Au and > 31T Au) (see Fig.11; Poulsen et al., 1996, see La Plata). Furthermore, VMS can be considered as Au-rich if the average gold grades (expressed

in ppm or g/t) exceed the combined content of base metals expressed in wt.% (Au g/t or ppm > Cu + Zn + Pb wt.%; Poulsen and Hannington 1996; Poulsen et al. 2000; Dubé et al. 2007). These deposits are formed in various submarine volcanic terrains (from bimodal mafic, bimodal felsic to bimodal siliciclastic) being present both on the recent seabed and in deformed and metamorphosed submarine volcanic settings (Dubé et al., 2007).

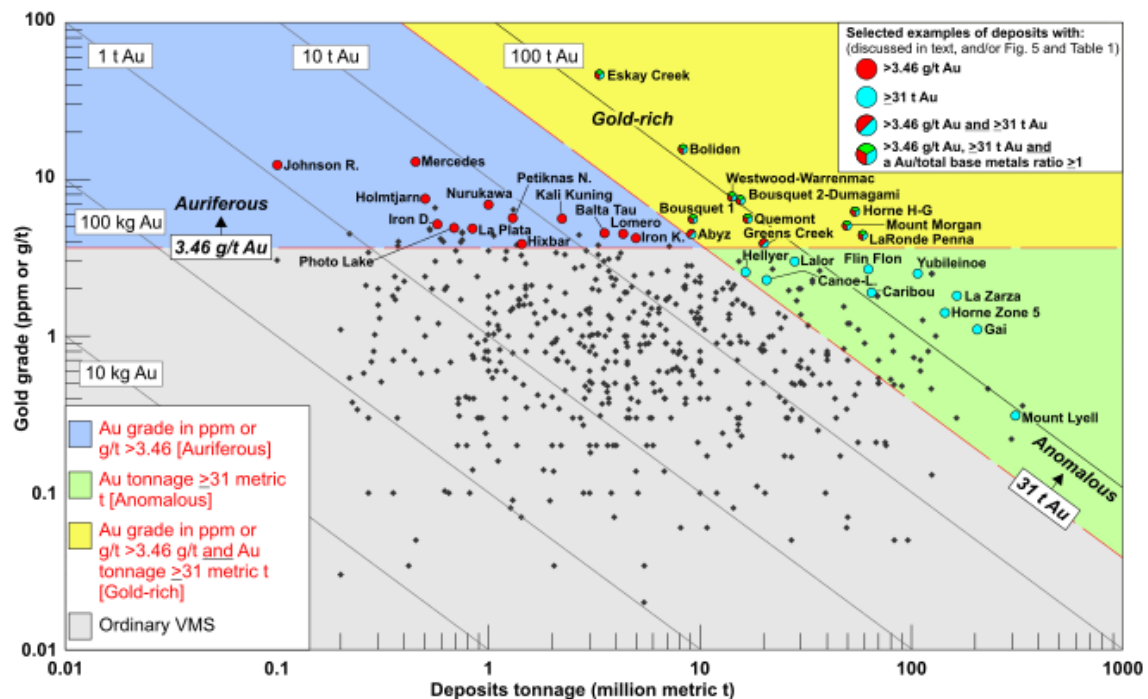


Figure 11. Bivariate plot of gold grade versus tonnage for VMS deposits. (Taken From: Mercier-Langevin et al., 2011).

These Au-VMS are equivalent to shallow-water submarine deposits and sub-aerial deposits of the epithermal clan, and can coexist with VMS poor in Au (see Fig 12; Sillitoe et al., 1996; Hannington et al., 1993; 1999). The tectonic setting of these deposits is associated with island arcs, fissured arcs, rear arc basins, or exterior arc fissures (striated arc) in modern volcanic environments (Hannington et al., 1999). The specific timing of formation of Au-rich deposits in certain VMS districts may be directly related to the geodynamic evolution of the arc-back-arc systems and the nature of the corresponding magmatism (e.g: Macuchi Arc in Ecuador; Chiaradia et al. 2008; Baimak-type VMS deposits of the South Urals; Prokin and Buslaev 1999; Herrington et al. 2005).

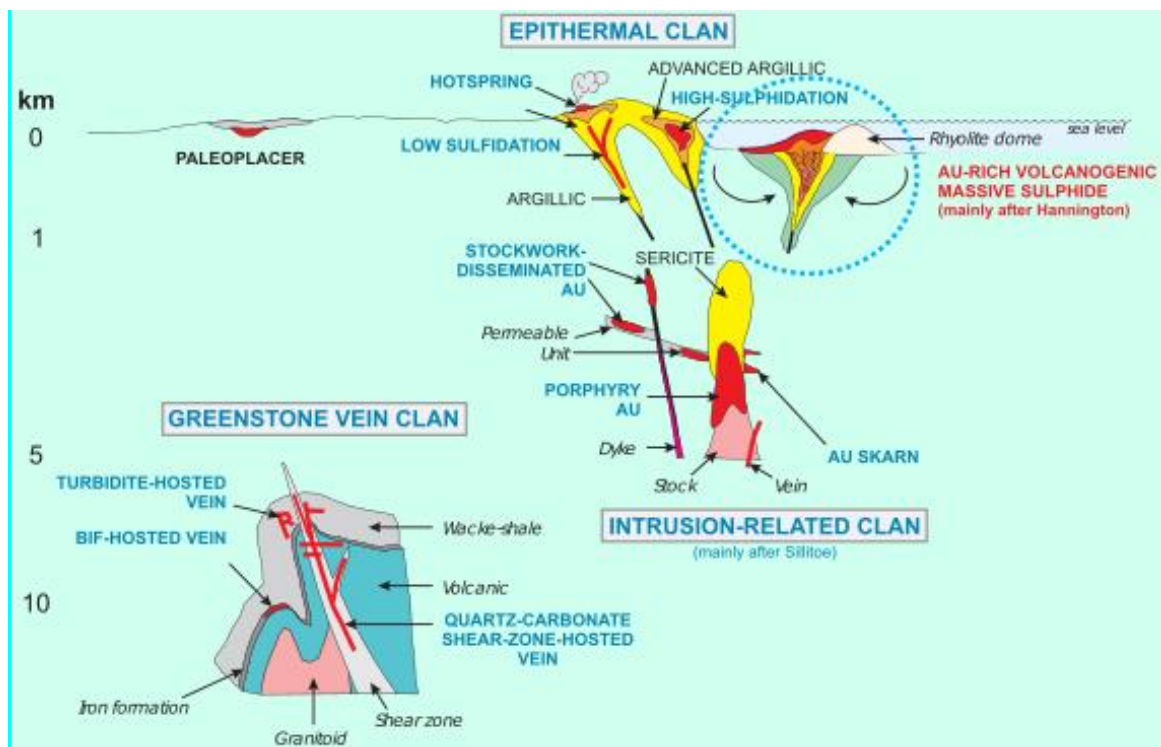


Figure 12. Schematic illustration of the various types of gold deposits shown at their inferred crustal levels of formation. (Taken from: Poulsen et al., 2000)

The Au-VMS deposits consist of a massive lenticular sulfide body with associated stock-work stringer feeders and discordant replacement zones (approx 2 km in vertical extension and tens of meters in the thickness of lenticular zones (Dubé et al. 2007). The bodies of the mineral are commonly tabular, stratiform and in bands associated with adjacent structures transposed by foliation into deformed and metamorphosed deposits (Dubé et al. 2007). In addition, the development of veins of syn-tectonic sulfide, parallel to the foliation in schist rocks, associated with alterations with quartz, white mica and sometimes aluminous silicates is evidenced (Dubé et al. 2007).

Au-rich VMS are associated with intermediate calc-alkaline to felsic transitional volcanic rocks (along with associated volcanoclastic products) and subvolcanic tonalitic intrusions near or at the interfaces with basalt-andesite or clastic sedimentary strata (Mercier-Langevin et al., 2011; Dubé et al. 2007). These deposits shows a massive silicic alterations (or with potassium feldspar in association with Au-Zn-Pb-Ag), advanced argillic (commonly in Au-Cu sub-class of Au-VMS). Also, it contains aluminous (indicative of an oxidized hydrothermal fluid low pH different from typical

near-neutral fluids) and trace element signatures such as Au, Ag, As, Sb, Bi, Hg and Te (suggesting direct magmatic input) (Mercier-Langevin et al., 2011; Dubé et al. 2007; Huston, 2000 add McClenaghan et al., 2009 on Louvicourt deposit from the Bathurst Mining Camp).

There are specific mineral associations in the Au-VMS deposits. The presence of quartz, serisite, and aluminous silicates (andalusite, kyanite, Zn-rich staurolite, and Mn-rich garnet) are typical in metamorphic greenstone terranes (Sillitoe et al., 1996; Huston, 2000). Au-VMS present distinct sulfide mineral associations such as pyrite and sulfides of base metal (chalcopyrite, sphalerite, galena) with a complex assembly of minor phases that include bornite, tenantite, sulfosalts, arsenopyrite, mawsonite and tellurides (Dubé et al. 2007). In pyrite and arsenopyrite, Au is housed as submicroscopic inclusions (1-5 microns) , or structurally linked in the crystal lattice (Adrienne et al., 1993; Huston, 1992). Furthermore, when pyrite formed under extreme conditions of temperature and pressure, it develops certain imperfections (dislocations) in the crystalline structure, which can be "decorated" with Au (Fougerouse, 2021). In addition, Au occurs as native metal and Au-tellurides in Cu-Au deposits, while polymetallic gold sulfides (Au-Zn-Pb-Ag) contain electrum that is often rich in Ag (Ag-Au 1: 2 to 10: 1) or mercury (Huston, 1992; Dubé et al., 2007; Hannington et al., 1999).

Deposition controls and tectonic re-mobilization produce an uneven distribution of Au (Dubé et al., 2007). Post-volcanic deformation and metamorphism cause re-mobilization of Au in faults, shear zones, and veins adjacent to sulfide lenses (Hannington et al., 1999). Au tends to be leached from the base and deposited at higher levels, lodging in massive sulfide lenses linked to strata, stockwork zone and disseminated sulfides (Dubé et al., 2007). The mobilization of metals produces variations in the zoning, thickness and proportions of the minerals defining the richest areas of the deposit (Huston, 2000). The re-mobilization of metals in Au-VMS produces low concentrations of Na, K and MREE and high concentrations of Cu, As, Mo, B, Te and RLEE in the proximal zone. On the other hand, the distal zone shows enrichment of Zn, Ca, Mn, C and epithermal suit of As, Sb and Hg (Dubé et al., 2007).

Some Au-VMS are characterized by scattered and / or economically more important semi-massive sulfide zones than massive sulfide zones due to a high degree of Au in the

stock-work zones, disseminations in barite lenses and exhalites located around of massive sulfide lenses (Hannington et al., 1999; Huston, 2000; Sillitoe, 1996; Scotney et al., 2005; Sewell & Wheatley et al., 1994). The occurrence of barite is greater in young deposits, locating it stratigraphically below or above the deposit together with caps rich in silica, sterile pyrite lenses or exhalites (Hannington et al., 1999).

5.2 Transport of Gold in mineralization systems

5.2.1 Chemical Affinity of Au

The oxidation states of Au (from +1 to +7) determine its ability to bind to anions and structurally substitute within minerals, Au^{+1} and Au^{+3} being predominant (Pokrovski et al., 2014). Gold-ligand is independent of T and P, confirming the covalent nature of the bonds and the coordination constancy of gold in a wide range of T and P. Au^{+3} is a strong and stable oxidant in environments surface oxidation while Au^{+1} is dominant in most hydrothermal fluids and silicate smelters. The low solubility, the formation of solid phases and Au colloids keep the high hydrolysis of Au^{+3} constant in a wide range from pH to ambient T. Au^{+3} in the solid and aqueous phase is always coordinated with 4 ligands in a square geometry, with the Cl^{2-} and OH^{2-} ions being the most common ligands to form complexes (Pokrovski et al., 2014).

Au^{+3} is limited to acidic groundwater and Fe^{+3} and Mn^{+4} oxyhydroxide mineral surfaces (Usher et al., 2009). The low temperature of well-oxygenated saline groundwater allows the preservation of Au^{+3} , since a rapid reduction of the Au^{+3} ion to Au^{+1} has been demonstrated after an increase in T in the acid complex $AuCl^{4-}$ (formed from Au^{+3} ion). In addition, the presence of reducing agents such as sulfides, organic matter or ferrous iron also promotes this reduction in aquatic systems. Acidic systems, such as the acid complexes of Au^{+3} , allow the precipitation and formation of minerals composed of $Fe(OH)_3$.

The Au^{+1} cation is a soft cation (large, weakly charged and easily polarisable) that forms linear structures of 2 coordinates, has hydroxide preference over the water ligand and hydrolyzes forming the neutral Au (OH) complex in a wide pH range (Berrodier et al., 2004; Vlassopoulos et al., 1990). Soft anions (such as HS^{-2} , CN^{2-} , $S_2O_3^-$ and Br_2^- have characteristics similar to soft cations, allowing the formation of covalent

complexes. Soft ligands such as SCN^- , CO_3^{2-} , and functional groups such as thiol and amide of fulvic and umic acids (produced by decomposition of algae and plants or by oxidation of pyrite and sulfur) are present. These soft ligands contribute to the transport of gold in surface waters (Adams, 2005) being an alternative to the use of dicyanide ($\text{Au}(\text{CN})_2^-$) for the selective extraction of gold from hydrothermal minerals.

5.2.2 Solubility and volatility of gold

Rol of physicochemical parameters

The variation of physicochemical parameters of the gas phase of volcanic systems determines the concentration of Au. The enrichment of Au in the vapor phase is due to the formation of volatile species with sulfur (S). In magmatic conditions with high sulfur content, the acidity of the system increases the distribution of Au together with its volatility and dispersion (Frank et al., 2011; Pokrovski et al., 2002, 2008). At high temperatures, diffusion of Au^+ is produced by vapor-type inclusions. The Au inclusions of the volcanic gas phase are immiscible in the vapor-liquid phase after the reduction of T and decompression of magmatic fluids upon surfacing (Hedenquist & Lowenstern, 1994; Heinrich et al., 1999; Kouzmanov & Pokrovski, 2020). Furthermore, the difference between the vapor density of volcanic gases near the surface and hydrothermal vapors also affects the solubility of Au and other minerals in the vapor phase (Pokrovski et al., 2014).

Rol of water pressure

Water pressure is essential in controlling the solubility of Au. The solubility of Au in the vapor phase determines three fundamental transport controls: 1) in the vapor-aqueous phase, Au forms a complex with ligands (especially with ions of Cl and sulfurs). 2) The vapor species in aqueous solution or dense supercritical fluids isn't charged, favoring the association of Au ions. 3) The increase of P in a vapor-solid system increases the dissolution of metals (Pokrovski et al., 2014). Sublimates collected in fumaroles of active volcanoes such as Fossa (Italy), Colima (Mexico), Kudryavy (Kuril Islands) show Au concentrations that vary from 0.001ppb - 20ppb in native metals and alloys (Quisefit et al., 1989).

Solubility and stability of Gold controlled by Fe, H_2S , HCl

The solubility and stability of Au preserves in systems rich in H₂S. Transport of 100-1000 ppm of Au in Au (HS)²⁻ and other complexes of sulfide and polysulfides in porphyry has been demonstrated (Seo et al., 2009, 2011; Tomkins, 2010). In epithermal environments (≤ 350 ° C), the solubility of Au is conditioned by the amount of ferrous Fe in the fluid and the rock (source of HS in the form of pyrite) (Richards, 2011; Sillitoe, 2010). In systems with reduced pressure, the high concentrations of H₂S dissolved in equilibrium with FeS favor the solubility of Au. Furthermore, in the vapor phase with decreasing pressure, the uncharged hydrogen chloride (HCl) or sulfide (H₂S) complexes retain the solubility of Au (Hedenquist & Lowenstern, 1994; Heinrich et al., 1999; Kouzmanov & Pokrovski, 2020).

Systems rich in sulfur

In systems rich in sulfur, the volatility of Au increases depending on the stability of the Au (HS) and AuHSO species against chlorides under acidic conditions (Pokrovski et al., 2002, 2008). The high volatility of Au in magmatic conditions compared to hydrothermal conditions is explained by the formation of hydroxide species (AuOH) or HCl (AuHCl₂) both in steam and in brine (Simon et al., 2005). Low concentrations of Au in HCl-rich volcanic gases prevent the formation of complexes such as Au₂Cl₂ and Au₂Cl₆ (Hager & Hill, 1970; James & Hager, 1978). Furthermore, the instability of the Au⁺³ chloride complexes in natural volcanic systems generates the dominance of complexes formed by Au⁺ (Pokrovski et al., 2014). Under epithermal conditions, the buffering of fluids by rocks or carbonates of alkali and alkaline earth aluminosilicates produces a pH of 5 to 7, which is favorable for the transport of Au in the form of Au (HS)²⁻ (Pokrovski et al., 2014). At high temperatures (porphids), the interaction with rocks neutralizes the acidic fluids, producing the decomposition of AuCl₂⁻ and the precipitation of Au (Pokrovski et al., 2014).

The presence of Iron

The presence of Fe intervenes in the behavior of Au in neutral silicate melts and degassing of volatile aqueous phases. The maximum solubility of Au and sulfide-sulfate redox transport is reached during the decomposition and dissolution of Fe sulfides, which supply a greater amount of reduced S to the melt (Pokrovski et al., 2014). However, in aqueous magmatic fluids containing Cl, S, FeS and Cu (from 100-10000

ppm), water and anhydrous silicate melts decrease the solubility of Au, forming oxides, sulfides or chlorides species with affinity to Au⁺ (Pokrovski et al., 2014).

Rol of CO₂ volatil

CO₂ is a common volatile component of fluids and vapors in Au deposits with molten silicates (Diamond, 1990; Hanley & Gladney, 2011; Phillips & Evans, 2004; Vallance et al., 2009). The presence of CO₂ provides the fluid with numerous characteristics such as: a) CO₂ affects the vapor-liquid phase relationship, increasing the early separation of phases, producing the fractionation of Au in systems rich in sulfur (Pokrovski et al., 2014). b) CO₂ is a weak acid that influences the pH of fluids and the solubility of Au. In high-pressure environments, high CO₂ reduces the pH to 5, allowing maintaining high concentrations of Au of the Au (HS)²⁻ form. However, in fluids rich in salt and at high T (> 400 ° C typical of porphyry) the effect of CO₂ on pH does not affect the behavior of Au (Pokrovski et al., 2014). c) The solubility of gold in the form of uncharged sulfur complexes increases the fraction of CO₂ in the fluid. d) CO₂ intervenes in the phenomenon of solvation in the fluid phase, increasing the solubility of the metal. However, in Au deposits such as porphyry, epithermal and Carlin (which have 10% mol CO₂), the solvation effect on Au transport is lower (Pokrovski et al., 2014).

5.2.3 Vapor-liquid transport of gold

The formation of sulfur complexes intervenes in the hydrothermal transport mechanism of Au. Sulfur carrier solutions intermediates such as polysulfide and thiosulfate complexes have affinity for Au⁺ ions. Thiosulfate intervenes in the mobilization of Au during oxidation at low temperatures of sulfur minerals, for example the concentration of thiosulfate in geothermal springs at T < 100 ° C reaches values comparable to those of H₂S, binding Au and similar metals. However, it tends to decompose into native sulfates and sulfur due to its instability at acidic pH (Kaasalainen & Stefánsson, 2011; Migdisov & Bychkov, 1998; Nordstrom et al., 1998).

The transport of metals by sulfuric fluids depends on the acidic conditions as they pass through the rock. Gold polysulfide complexes (AuSnS²⁻) form at moderate temperatures of approximately 100-150 ° C and compete with HS for Au during its transport in active and epithermal geothermal systems near the surface (Palyanova et al., 1993; Pokrovsk

et al., 2014). Hydrogen sulfide complexes form monohydrogen sulfide (AuHS) species under acidic conditions and Au (HS)²⁻ bi-hydrogen sulfide species at neutral to basic pH, generating different Au precipitation potentials in these fluids (Pokrovski et al., 2009, 2014). The massive transport of Au (HS)²⁻ occurs at T 150-200 ° C, producing a greater potential for economic precipitation of Au when H₂S is diluted, oxidized or lost through interactions with rocks containing Fe (Pokrovski et al., 2014).

5.3 Occurrence of Gold in minerals

5.3.1 Gold precipitation processes

Magmatic, hydrothermal, and metamorphic fluids containing Au go through five main processes that cause the redistribution and deposition of Au and associated metals: cooling, decompression, fluid-rock interaction, phase separation, and fluid mixing (Pokrovski et al., 2014).

Cooling

Temperature influences the solubility, transport and precipitation of metals. Thermodynamic models show that the cooling of an acidic saline fluid is an efficient mechanism for the deposition of Au (together with quartz and pyrite) in veins (Garrels, 1968). The precipitation of pyrite and chalcopyrite in sulfur fluid systems with excess iron ferrous (and copper) causes the precipitation of Au (Pokrovski et al., 2014). The rapid cooling of a saline fluid removes all the H₂S in the form of metal sulfides, allowing the deposition of Au together with other metals (Cu-Zn-Pb) and iron sulfides on the seafloor (Candela, 2004). AuCl₂ at 500 bar produces a deposition of 95% of Au after a drop of 50 ° C (within the range of 500-300 ° C) (Williams-Jones et al., 2009). In the vapor phase enriched in H₂S, Au is transported in sulfide species volatiles up to 150-200 ° C without precipitation (Pokrovski et al., 2014).

Decompression

The decrease in pressure in a single-phase fluid can also affect the solubility of Au. In addition, pressure changes associated with fractures and cracks in the rock are significant in the deposition of gold and quartz (Boyle et al., 1969)

Phase Separation

In magmatic and hydrothermal systems, phase separation occurs due to the coexistence of liquid and vapor inclusions (Pokrovski et al., 2014). In epithermal environments, separation occurs when dilute aqueous liquid boils, forming vapor bubbles (Pokrovski et al., 2014). Phase separation at high T - P tends to fractionate metals such as As, S and Au (and partially Cu) in the phase vapor compared to Fe, Zn, Pb, Ag (see Fig 13; Pokrovski et al., 2014). Furthermore, in low temperature epithermal environments (350-300 ° C), Au does not participate significantly in low density vapor phases (Pokrovski et al., 2014).

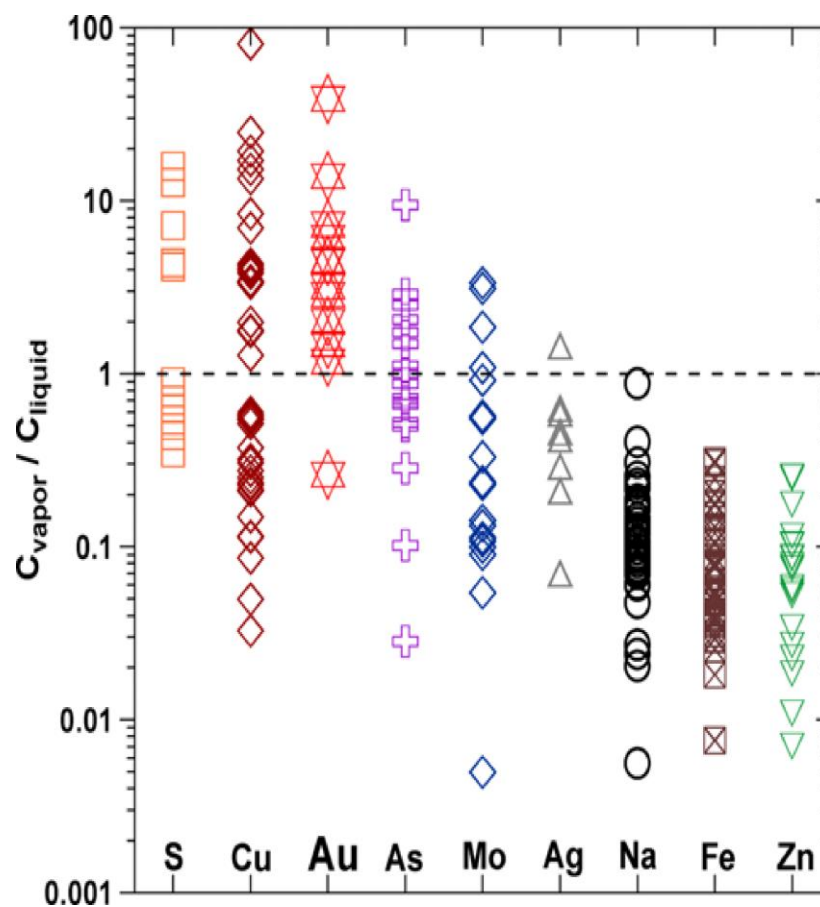


Figure 13. Concentration ratios for sulphur, gold, and associated metals measured in coexisting vapor and hypersaline liquid inclusions from boiling assemblages in quartz from porphyry Cu–Au–Mo and related deposits. (Taken From: Pokrovski et al., 2014).

The effect of liquid boiling in low-temperature epithermal systems is the elimination of H_2S and CO_2 in the vapor, decomposing Au-hydrogen sulfide complexes and precipitating Au (Saunders & Schoenly, 1995; Simmons et al., 2005). The high CO_2 content increases the mobilization of metals in the system favoring phase separation at decreasing depths of formation (Mikucki, 1998). Boiling increases the pH by breaking up the acid components in the vapor, increasing the deposition of Au (Williams-Jones et al., 2009). Additionally, the flow of focused fluids (systems with high impermeability) and the efficient deposition of Au induced by boiling are two key factors for the formation of large epithermal Au deposits (Simmons and Browne, 2007).

Fluid-rock interactions

The slow interaction of fluids with the rock produces changes in pH and sulfide content, being the main mechanism of formation of deposits rich in Au (Boyle, 1969). In mafic rocks rich in minerals with ferrous iron (olivine-pyroxene), hydrothermal fluids rich in S tend to react and precipitate S minerals, decreasing the concentration of H_2S (Pokrovski et al., 2014). The hydrothermal alteration of the rock implies pyritization and the gold-pyrite relationship in mesothermal (orogenic) deposits (Pokrovski et al., 2014). In addition, the oxidation reaction between hydrothermal fluids and hematites of the box rock increases pO_2 , favoring the reduction of HS^- and the solubility of Au (Williams-Jones et al., 2009).

Fluid mixing

The mixture of two fluids with different temperatures, acidity or composition induces the formation of Au-bearing minerals in crust environments close to the surface, such as hydrothermal systems on the seabed (Candela, 2004). $HCl-H_2O$ mixtures in the gaseous state (with T from high sulfidation systems) are capable of dissolving more than 10 ppb of Au in epithermal systems, forming $AuCl (H_2O)_{3-5}$, $AuS (H_2S)_2$ and $AuS (H_2S)_3$ (Archibald et al., 2001).

5.3.2 Gold in sulfide minerals

The precipitation of metals in aqueous complexes of Au-As-S (+ Sb, Se, Te) is produced by the presence of FeII, favoring the formation of minerals in the system

(Boiron et al., 1989; Boyle, 1969). Studies related to Arsenian pyrite determined the presence of Au in two forms: Au in nanometric size and Au chemically bound with an uncertain oxidation state (Arehart et al., 1993; Boiron et al., 1989; Boyle, 1969; Cabri et al., 2000; Palenik et al., 2004; Reich et al., 2005; Scaini et al., 1998; Simon et al., 1999). Gold emplacement occurs at concentrations ranging from a few ppm to 1000 ppm in pyrite and arsenopyrite state (Arehart et al., 1993; Cabri et al., 2000; Palenik et al., 2004; Reich et al., 2005; Scaini et al., 1998; Simon et al., 1999). Factors such as fluid cooling or boiling are favorable for the precipitation of pyrite / arsenopyrite together with Au (Velásquez et al., 2014). Pyrites rich in arsenic with Au / As ratio lower than 0.02 have the dominant form of Au⁺ while those higher than 0.02 have significant fractions of Au nanoparticles.

Chapter 6: Macuchi VMS deposits

The massive sulfide deposits of Macuchi Formation are Kuroko/Noranda type VMS deposits (see Fig.1) with unusual Au content. Among these deposits, the most important ones are “El Domo” (2.99g Au / t) and “La Plata” (12.9 g Au / t) are Cu-Zn type (see Fig.14) (Vallejo et al., 2016). The enrichment of gold in these deposits depends on the formation system of the VMS deposits in this tectonic setting, the type of metal enrichment, and the subsequent tectonic re-mobilization (McClenaghan et al., 2009). The analysis of these data together with those already obtained from mining companies (technical reports) will consolidate a base knowledge for future prospecting, exploration and exploitation strategies of these deposits, and possibly similar deposits in the neighboring Andean region.

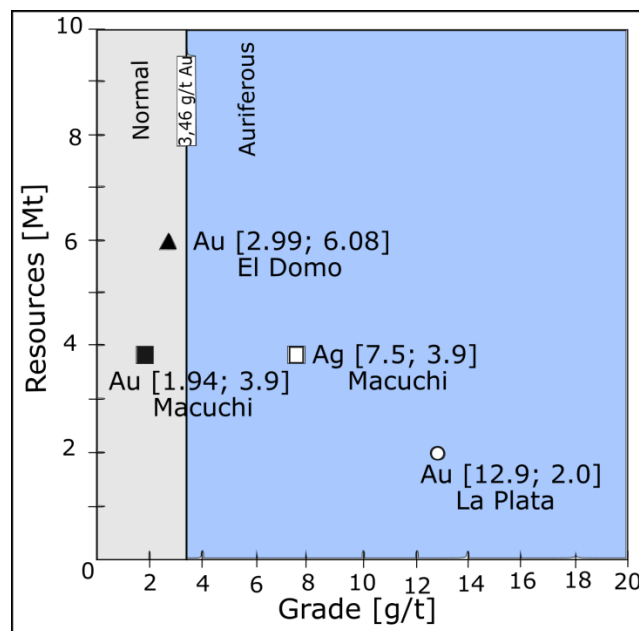


Figure 14. Grade vs. Resources chart for Macuchi VMS deposits (From: Toro Álava J, 2021; Mercier-Langevin, 2011).

The VMS deposits of the Macuchi Formation are associated with an oceanic setting formation. The subduction of the Piñón oceanic plate enhanced the accretion of oceanic terrains in Western Ecuador during the Miocene (Chiaradia et al., 2003). The subduction of this oceanic crust, previous to accret oceanic terrains, formed an island arc and allowed the increase of magmatism in this unit. The magmatic activity in the back-arc of the island arc (Fig. 10) enhanced hydrothermal fluids rising into shallow marine levels and form the VMS deposits (Chiaradia et al., 2004a, 2004b; Mercier-

Langevin et al., 2011; Schutte, 2010). Three VMS deposits of economic importance reported from the Macuchi Formation, including, “Macuchi”, “La Plata”, and “El Domo” (Fig. 1).

6.1. Macuchi Formation

The set of increased oceanic plateaus (Pallatanga Fm) form the basement of the Western cordillera mountain range, the Coastal Zone and the floor where the Macuchi Formation (MacuchiFm) was deposited (Vallejo et al., 2006; 2016). The oceanic plateaus, formed by volcanic plumes, fed from the lower mantle (Saunders et al. 1996), generating special conditions of thickness and mineralogical composition that favor their buoyancy and hinder their subduction (Vallejo et al., 2016). Pallatanga Fm collided with South America during the Campanian-Maastrichtian period (Spikings et al. 2005; Luzieux et al. 2006; Vallejo et al. 2006), deforming the continental margin and synchronously forming the Pallatanga fault during accretion (Litherland et al. 1994; Spikings et al. 2001; Vallejo et al. 2016).

The presence of Cambrian zircons in the Macuchi Fm (Vallejo et al. 2009) and the accretion union of the allochthonous basement of the Coastal Region (to the Western Cordillera during the Cretaceous (Spikings et al. 2005; Luzieux et al. 2006; Vallejo 2007) suggested the formation of the Macuchi arc along the basement of the Western Cordillera (Chiaradia et al., 2004; Vallejo et al., 2016). The recrystallized limestone in the unit defines the Macuchi Island Arc as a low latitude arch with peripheral reef systems (Hughes & Pilatasig, 2002; Vallejo et al., 2016). The analysis of volcanic rocks from Macuchi Fm shows a volcanic arc formed by basalt, andesite, dacite and calco-alkaline riodacite high in K₂O (Hughes and Pilatasig 2002; Vallejo 2007; 2016; Vallance et al., 2009). The variability of compositions in this formation is explained by the mixture between primitive magmas from the mantle and hybrid magmas (intermediate to felsic) formed in the lower part of the oceanic plateaus (Chiaradia and Fontboté, 2001; Vallance et al., 2009).

The Macuchi formation is composed of pillow basaltic lavas, lithic tuffs (basaltic and andesitic), basaltic breccias, andesitic intrusions, volcanic material reworked in turbiditic beds and cherts (Cuenca, 2012; Vallejo, 2007) with a thickness greater than 2

km (Kerr et al., 2002; Vallejo et al., 2016). Most of the formation consists of mafic rocks (volcanoclasts) deposited in a succession of submarine volcanic arc during the Paleocene to the late Eocene (Aguirre and Atherton, 1987; Egüez, 1986; Spikings et al., 2005; Vallejo, 2007). The rocks of the formation include angular to sub-rounded clasts of basalts, andesites, riodacites, and dacites in a glass-rich epidotized andesite groundmass (Vallejo et al., 2016). Furthermore, the unit shows low-grade metamorphism characterized by zeolite, prehnite-pumpellyite, and greenschist assemblages (Aguirre and Atherton, 1987).

6.2 El Domo Deposit

El Domo is located to the west of the western mountain range of Ecuador, 180 km southwest of Quito, in the Macuchi formation (Paleocene-Eocene)(Hughes & Pilatasig, 2002). El Domo has 6.080Mt with 2.99g / t of gold, considered as the largest VMS deposit in the northern Andes (Calvo & Johnson, 2014) El Domo deposit was formed by magmatic-hydrothermal discharge in separation basins, produced by local stress regimes (Vallejo et al., 2016). It forms a lens of massive sulfide with irregular and stratified edge 15-20m thick, 150m wide and 550m long, housing 95% of the resource (Vallejo et al., 2016).

Porosity and reactivity of mafic (glass-rich) and felsic rocks created site by mineralization (massive to disseminated) at a depth of 10-20 m below the seabed (Vallejo et al., 2016). The shallow depth is evidenced through clasts with massive sulfide within the higher volcanoclastic horizons and by the absence of mineralization or alteration in the debris flow (Vallejo et al., 2016).

The footwall sequence is inclusive of late andesite cryptodomes and basaltic dikes with varying degrees of hydrothermal alteration (see Fig. 15; Vallejo et al., 2016).

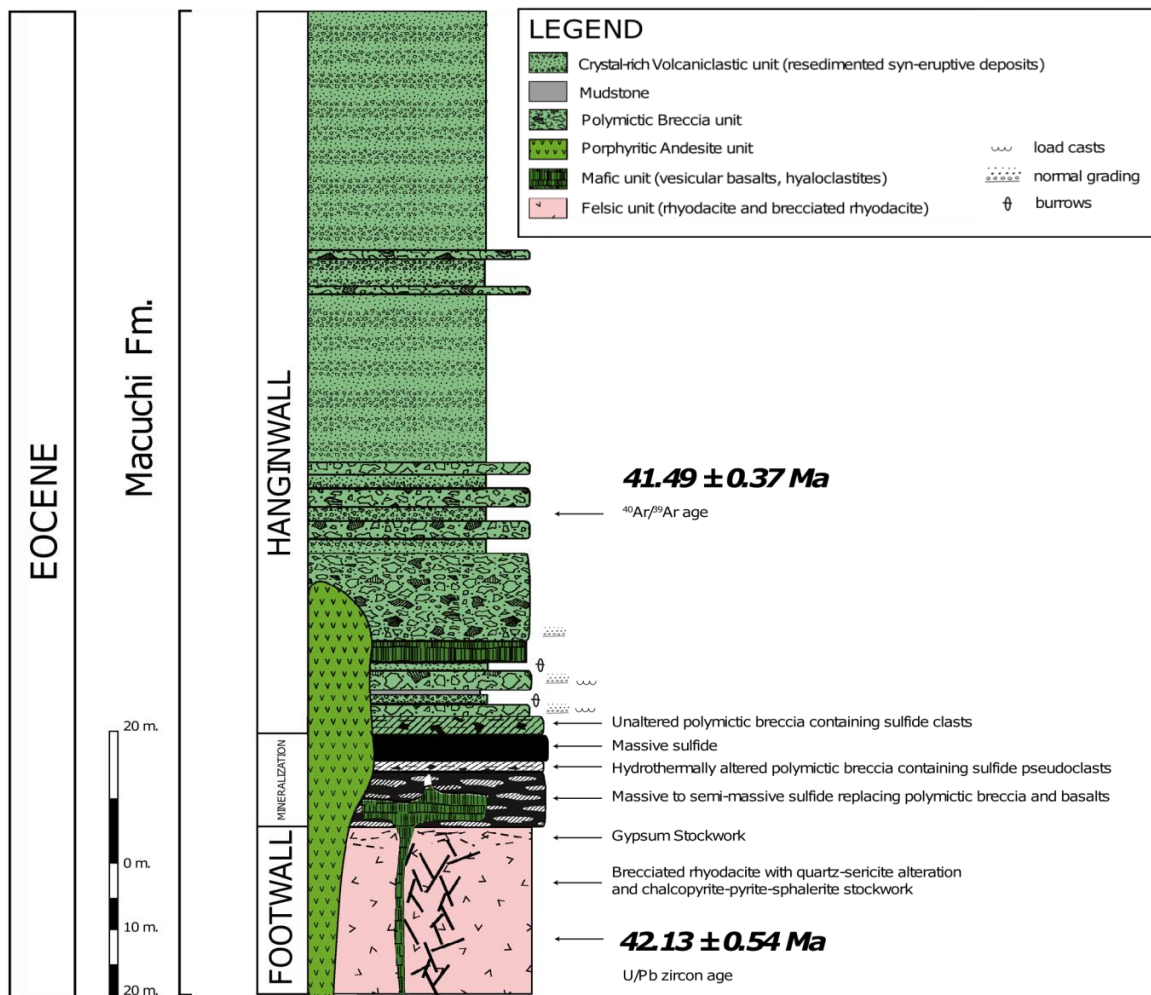


Figure 15. Stratigraphy of the El Domo area, including the massive sulfide zone (Taken From: Vallejo et al., 2016).

Isotopic and geochemical data suggest that the thick naturalness of the basement to the Macuchi formation produced hybrid and intermediate to felsic magmas that form the footwall of the Domo. The felsic unit is composed of ancient felsic volcanic rocks with a predominance of rhyodacite (coherent and brecciated). The coherent riodacite is located in distal zones while the breccias in proximal zones to the massive sulfide (Vallejo et al., 2016). The unit consists of plagioclase and quartz phenocrysts interspersed with autoclastic and transported breccias and in-situ hyaloclastite. The rhyodacite footwall harbors areas of irregular stringers (quartz-beingsite-pyrite alteration). The footwall of El Domo was created from hybrid magmas, intermediate to felsic due to the thick nature of the basement of the Macuchi formation (Vallejo et al., 2016). On the other hand, the volcanoclastic lithologies of the hangingwall exhibit silicification, chloritization, and argillization (Vallejo et al., 2016).

The polymictic gap unit of the hangingwall overlaps the felsic unit. It is composed of breccia beds supported by heterogeneous clasts with chaotic polymictic fragments (Vallejo et al., 2016). The composition of clasts includes plagioclast-coherent phyrlic andesite, volcanic mafic sandstone, riodacite, quartz-rich rhyolite, aphyric basalt with scattered pyrite, and red jasper (Vallejo et al., 2016). Meter-thick breccia beds are interspersed with thicker layers of rolled shale and volcanic glass sandstones. Sedimentary structures show sequences of turbidites with erosive bases (Vallejo et al., 2016).

The hangingwall mafic unit is dominated by massive basalt (20m) with an aphyric texture with scarce phenocrysts (plagioclase, pyroxene and olivine) present between layers with the massive sulfides (Vallejo et al., 2016). The texture and transverse relationships of the mafic unit describe an underwater lava flow with subvolcanic dikes (Vallejo et al., 2016). The crystal-rich volcanoclastic unit of the hangingwall is characterized by thick breccia body units with homogeneous plagioclase-andesite fragments covered by sandstones and shales (Vallejo et al., 2016). The porphyritic andesitic unit of the hangingwall is located on the periphery of the deposit, contains andesitic domes that cut through the volcanic rocks of massive sulfide and hangingwall. Andesite invades older units breaking host rocks (including the VMS) on the eastern edge of reservoir (Vallejo et al., 2016). Hangingwall mafic inclusions show abundant high-level holocrystalline (basaltic-microgabbroic) dikes traversing felsic rocks (Vallejo et al., 2016). Holocene deposits consist of gravity-driven debris flows supported by matrices from local and distal sources (Vallejo et al., 2016).

The mineralization of the dome includes massive and semi-massive sulfides located between the submarine rhyodacitic dome complex and on mafic rocks and hydrothermally altered volcanoclastic sediments rich in glass (Schandl, 2009; Vallejo et al., 2016). The volcanic sequence harboring the massive sulfides dated from $^{40}\text{Ar} / ^{39}\text{Ar}$ of 41.49 ± 0.37 Ma, while the riodacite from the footwall dates from Zr U-Pb 42.13 ± 0.54 Ma for the interval of mineralization (Vallejo et al., 2016). Mafic rocks have typical VMS district tholeiitic affinity, while felsic rocks show a calcalkaline sequence (Vallejo et al., 2016).

The stockwork characterizes by massive pyrite and regularly replaced by chalcopyrite (Vallejo et al., 2016). There is a Cu-rich zone dominated by Fe-rich sphalerite with sulfides of Cu, As, and Ag (chalcopyrite, bornite, tenantite, stromeyerite, and proustite) (Vallejo et al., 2016). The zone rich in Zn-Pb (mainly sphalerite and galena) covers the zone rich in Cu forming a polymetallic boundary (Vallejo et al., 2016). The polymetallic mineral contains most of Au and Ag. Au in grain (5-50 um) is almost pure within fractures in sphalerite, while Ag (10-100 um) is in stromeyerite and proustite (see Fig.16; Schandl, 2009). The stringer zone is made up of quartz “betas” with pyrite and, to a lesser extent, chalcopyrite, sphalerite, and galena (with the presence of gypsum) (Vallejo et al., 2016).

The footwall zone has phyllic alteration (quartz-beingsite and pyrite) with chlorites, illites and smectites surrounded by a halo of smectite-chlorite alteration (Vallejo et al., 2016).

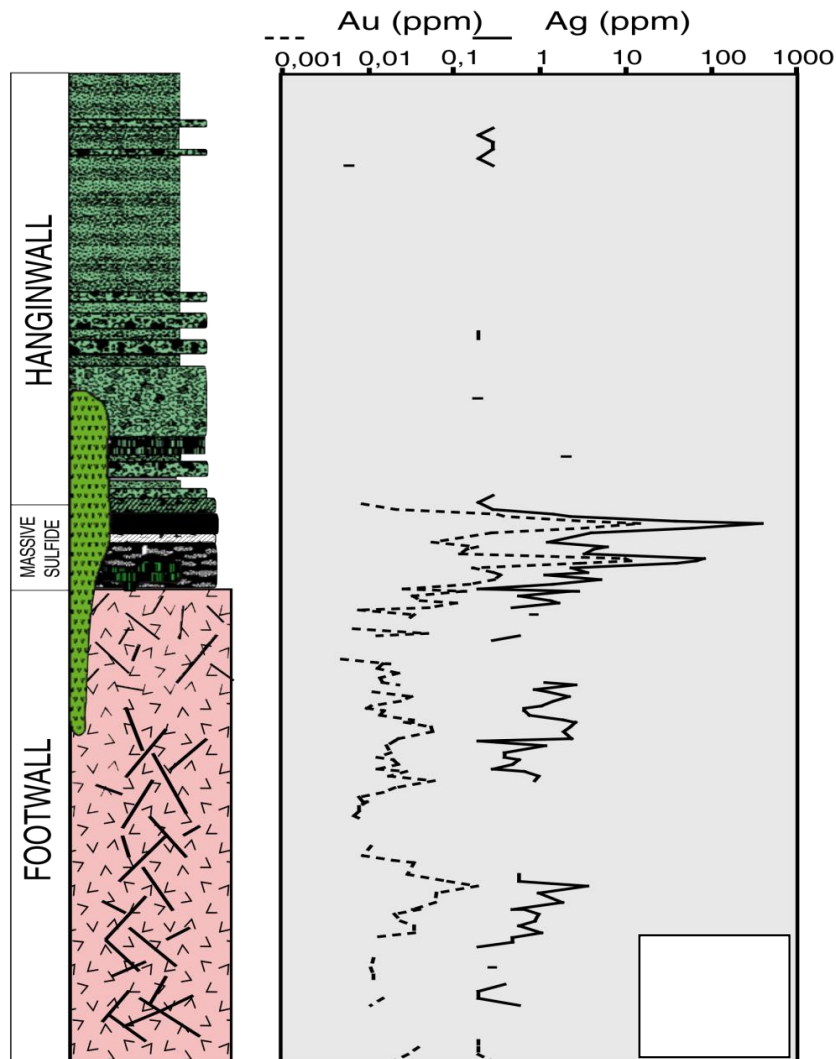


Figure 16. Au and Ag concentrations in El Domo VMS deposit (Taken From: Vallejo et al., 2016).

The faults facilitated the formation of volcanic rock deposits and the control of the hydrothermal system (Vallejo et al., 2016). The deformation created an NNE-SSW separation basin bounded by the Pallatanga and Chimbo-Toachi fault system (Vallejo et al., 2016). The deposit cut rocks that present brittle foliation with fragments of altered rhyodacite within a mass of quartz, sericite, and locally foliated gypsum (Vallejo et al., 2016).

6.3 La Plata Deposit

The La Plata (formerly called La Mina) deposit is located 57km southwest of Quito and 32km southeast of Santo Domingo de los Colorados (Chiaradia et al., 2003). A content

of 2Mt is estimated with 12.9g / t of Au, considering an Au–VMS. This VMS deposit contains massive and semi-massive sulfide lenses 10m thick and 100m of lateral extension (Chiaradia et al., 2003).

The footwall is composed of altered dacite cut laterally by mineralized stockwork. The pearly textures of the footwall show volcanic submarine environments. The hanging wall is formed by massive, brecciated basaltic to andesitic volcanic rocks (Chiaradia et al., 2003).

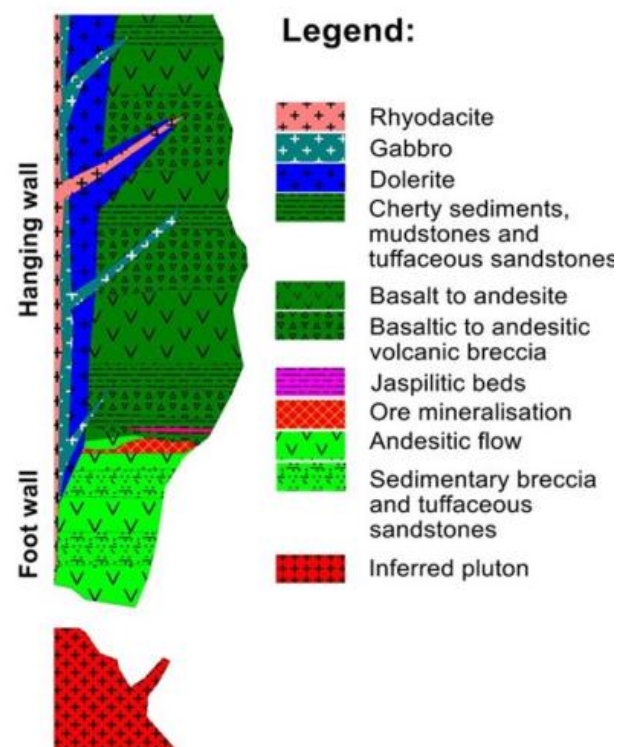


Figure 17. *Lithostratigraphic sequence of the La Plata.* (Taken from: Inc, 2019)
The main sulfide mineralization in La Plata is found on the eastern anticline flank between felsic and mafic rocks (Chiaradia et al., 2003). The mineralization and the host sequence show low-grade metamorphism (zeolite facies) (Chiaradia et al., 2003). Mineralization stages at the La Plata VMS are: a) Deposition of initial stage of the mineral where massive pyrite. b) Main stage of the mineral characterized by deposition of economic minerals (chalcopyrite, sphalerite, bornite and galena). c) Late stage where there is an abundant barite precipitation (see Fig.17; Chiaradia et al., 2003). The main Au minerals are: chalcopyrite, pyrite, sphalerite, bornite and galena (see Fig.18), showing Au grains with 5-350 um (Chiaradia et al., 2003).

Stages	Early ore stage	Main ore stage	Late ore stage
<i>Pyrite</i>	—————		
<i>Bornite</i>		—————	
<i>Sphalerite</i>		■ ■ ——— ■ ■	
<i>Fahlore</i>		- ———	
<i>Galena</i>		- - - ———	
<i>Digenite</i>		-----	
<i>Chalcocite</i>		-----	
<i>Chalcopyrite</i>		—————	
<i>Covellite</i>		-	
<i>Gold</i>	-	-	
<i>Barite</i>	- - -	- - - - -	—————

Figure 18. Paragenetic mineral sequence at the La Plata deposit. (Taken from: Chiaradia et al., 2003).

The hydrothermal alteration of the footwall shows quartz, sericite, pyrite, ± chlorides, ±illite, while the alteration in the hanging wall shows: hematite, pyrite, bornite±ankerite (Chiaradia et al., 2003).

6.4 Macuchi Deposit

Macuchi contains two parallel trends of massive sulfides that extend over a break zone of more than 6 km. The western trend is from San Carlos to Minchoa and the eastern trend is from La Esperanza to El Patiño. The Macuchi deposit is a massive Au-Cu sulfide center with an important stringer zone. Largo Resources is a mineral resources exploration and development company that is in charge of the 65,000 hectare Macuchi Gold Belt project with inferred mineral resources of 3.9 Mt grading 1.94g / t Au, 7.5g / t Ag. The program Drilling was 20 holes in extensive and broad areas of sulfide mineralization, with significant polymetallic values, in a massive volcanic epithermal sulfide environment.

Chapter 7: Conclusions and recommendations

7.1 Conclusions

The Macuchi formation formed in a submarine volcanic arc adjacent to the basement of the eastern mountain range. Stratigraphic, geochemical, thermo-chronological, and paleomagnetic studies demonstrated that the allochthonous basement of the Coastal Zone was already attached to the Western ridge since the Late Cretaceous. The presence of zircons (late Cambrian) in the Macuchi Formation suggests the formation of the Macuchi arc along the basement of the eastern mountain range.

Oblique convergence in the northern Andes formed a pull-apart basin and transcrustal faults that controlled the mineralization of the VMS deposits at Macuchi. The Pallatanga and Chimbo-Toachi faults are the result of a realizing bend system and accretion events on the continental margin during the Eocene. The local extension and fault systems could favor the magmatic and hydrothermal activity in the area creating the VMS deposits.

Factors that control solubility and volatility of gold are: 1) Physicochemical parameters; 2) Water pressure; 3) Control by Fe, H₂S, HCl; 4) Control of Sulfur; 5) Presence of Iron; and 6) Rol of CO₂ volatile. Precipitation of gold is controlled by: 1) Cooling; 2) Decompression; 3) Face separation; 4) Fluid-rock interactions; and 5) Fluid mixing.

Regarding the chemistry of Au complexes of Au (OH), AuCl₂, Au (HS), and Au (HS)₂ are dominant in aqueous hydrothermal solutions. Other complexes involving different forms of S, Cl, alkali metals, can operate in fluids, vapors and melts rich in S at high T. Au has a high affinity for reduced sulfur, which produces an enrichment of Au in vapors rich in S and molten sulfides, being an important source of Au in hydrothermal deposits. CO₂, sulfides and arsenic affect the concentration of Au, and the transport, precipitation and fractionation of other metals.

There are processes that influence the behavior of Au in the crust. Au is soluble in aqueous solutions of Na (HS), due to the complexes of Au with which Au (HS) and Au (HS)₂ species form. Au dissolves in a higher percentage in mixtures of Cl (except in HCl gas) and steam. On the other hand, in aqueous liquids, Au is dissolved in solutions

of Cl^- or HS^- (considered the most important ligands in the transport of Au) in significant quantities exceeding 1000ppm at 300 ° C.

Deposits > 3.46g / t are considered gold-bearing, > 31 t Au are considered to be anomalous in terms of Au content regardless of grade. Deposits of > 3.46g / t and > 31 t are Au rich VMS. VMS rich Au associates with intermediate to felsic calcalkaline transitional volcanic rocks that may reflect a geodynamic environment.

El Domo deposit has a content of 6.08 Mt with a grade of 2.99 g / t of Au. El Domo is a normal VMS deposit that has a massive sulfide lens 15 to 20 m thick and 550 m long. The footwall contains a unit felsic composed of riodacite, plagioclase phenocrysts and quartz. The hangingwall is composed of different units such as the polymictic breccia unit composed of breccia beds supported by heterogeneous clasts with chaotic polymictic fragments, the mafic unit dominated by massive basalt with firm texture, the Crystal-rich volcanoclastic unit, the porphyritic andesitic unit containing andesitic domes and finally mafic inclusions showing abundant holocrystalline dikes. In sulfide mineralization, the stockwork is made up of massive pyrite, a Cu-rich zone and a Zn-Pb-rich zone (mainly sphalerite and galena), while the stringer zone is made up of quartz “betas” with pyrite. It has a phyllic alteration (quartz-beingsite and pyrite) with chlorites, hillites and smectites surrounded by a halo of smectite-chlorite alteration. The deformation formed by repositioning the shallow seabed, without presenting large cut areas. However, it presents faults that cross the sequence but without significant deformations; this created a separation basin limited by the Pallatanga and Chimbo-Toachi fault systems.

La Plata VMS deposit has 2Mt with a grade of 12.9 g / t of Au, considered a rich Au - VMS; it has a massive and semi-massive sulfide lens 10 m thick and 100 m long. The Footwall contains felsic rocks ranging from riodacite to rhyolite, with pearlite textures, from underwater volcanic environments. The hangingwall contains massive volcanic rocks and brecciated basaltic to andesitic rocks. The mineralization of sulfides divides in three stages: a) Initial stage, where massive pyrite precipitated. b) Main stage, where the deposition of minerals such as chalcopyrite, sphalerite, bornite and galena takes place. c) Late stage, where there is abundant barite precipitation. The hydrothermal alteration of the footwall shows quartz, sericite, pyrite, \pm chlorides, \pm illite, while the

hangingwall shows hematite, pyrite, ersite \pm ankerite. The deformation is strong and presents large bodies of foliated catadasite, so they are synchronous, probably related to the movement of the regional Chimbo-Toachi fault.

7.2 Recommendations

- Relate the stratigraphies of the eastern zone of the Equator with logs electric from Petroecuador, Petroamazonas to evidence Sunsas and possible sedimentary analysis (drilling) to identify Grenville in the north of the country.
- To carry out drill, sample and detailed studies on the mineral composition and provenance of the Chaucha/Tahuin terrain, and the basement of the Eastern Cordillera to verify different theories or propose new studies regarding the Macuchi formation.
- A geodynamic setting analysis of Macuchi Fm, including genesis, accretion process and magmatism.
- Run more detailed study about the different zones of mineralization within La Plata deposit (Au-VMS) in which a higher grade and content of Au is evident. Due to the polymetallic content that VMS deposits present, it turns into economic potential within a market with fluctuating prices of metals.
- Define the mineral zoning of Macuchi VMS deposits, recognizing the main composition in these zones, size mineralization zones and grade of metals in it (Au, Ag, Zn, Cu & Pb) to determine formational patterns, zone refining occurrence, semi-permeable interfaces and larger and high grade zones.
- Macuchi VMS deposits belong to sub seafloor replacement kind of VMS. The identification of framboidal Py (acting as nuclei to generate first sulfide mineral precipitation) and its replacement in the breccias (massive sulfide zone), will allow to identify the kind of replacement that happened during the formation of these VMS deposits and its relation to the increased grades of metals.

References

- Adams, M. D. (ed.) 2005. *Advances in Gold Ore Processing*. Elsevier, Amsterdam.
- Adams, M. D. (2005). Summary of gold plants and processes. *Developments in Mineral Processing*, 15, 994-1013.
- Adrienne, Larocque, & Hodgson, J. (1993). Gold Distribution in the Mobrún Volcanic-Associated Massive Sulfide Deposit, Noranda, Quebec: A Preliminary Evaluation of the Role of Metamorphic Remobilization. *Economic Geology*, 88, 1443-1459.
- Aguirre, L., and Atherton, M.P., 1987, Low-grade metamorphism and geotectonic setting of the Macuchi Formation, Western Cordillera of Ecuador: *Journal of Metamorphic Geology*, v. 5, p. 473-494
- Allen, R.L., Weihed, P., and Global VMS Research Project Team, 2002, Global comparisons of volcanic-associated massive sulphide districts, in Blundell, D.J., Neubauer, F., and Von Quadt, A., eds., *The Timing and Location of Major Ore Deposits in an Evolving Orogen*: Geological Society of London Special Publication 204, p. 13-37.
- Archibald, S. M., Migdisov, A. A., & Williams-Jones, A. E. (2001). The stability of Au-chloride complexes in water vapor at elevated temperatures and pressures. *Geochimica et Cosmochimica Acta*, 65(23), 4413-4423. [https://doi.org/10.1016/S0016-7037\(01\)00730-X](https://doi.org/10.1016/S0016-7037(01)00730-X)
- Arehart, G. B., Chryssoulis, S. L., & Kesler, S. E. (1993). Gold and arsenic in iron sulfides from sediment-hosted disseminated gold deposits: implications for depositional processes. *Economic Geology*, 88(1), 171-185. <https://doi.org/10.2113/gsecongeo.88.1.171>
- Bartok, P. (1993). *Prebreakup of Gulf of Mexico-Caribbean and I NORTH location of the west central Pangea area of study . For Laurentia , abbreviations are T , (Yucatan); PIL Pinar been*. 12(2), 441-459.
- Benavides-Cáceres V (1999) Orogenic evolution of the Peruvian Andes: the Andean cycle. In: Skinner BJ (ed.) *Geology and ore deposits of the Central Andes*. SEG Special Publ 7:61-107
- Berrodier, I., Farges, F., Benedetti, M., Winterer, M., Brown, G. E., & Deveugèle, M. (2004). Adsorption mechanisms of trivalent gold on iron- and aluminum-(oxy) hydroxides. Part 1: X-ray absorption and Raman scattering spectroscopic studies of Au(III) adsorbed on ferrihydrite, goethite, and boehmite. *Geochimica et*

Cosmochimica Acta, 68(14), 3019–3042.
<https://doi.org/10.1016/j.gca.2004.02.009>

Beutel, E. K. (2009). Magmatic rifting of Pangaea linked to onset of South American plate motion. *Tectonophysics*, 468(1–4), 149–157.
<https://doi.org/10.1016/j.tecto.2008.06.019>

Boiron, M. C., Cathelineau, M., & Trescases, J. J. (1989). Conditions of gold-bearing arsenopyrite crystallization in the Villeranges basin, Marche-Combrailles shear zone, France: a mineralogical and fluid inclusion study. *Economic Geology*, 84(5), 1340–1362. <https://doi.org/10.2113/gsecongeo.84.5.1340>

Boland, M.P., McCourt, W.J., Beate, B., 2000. Mapa geológico de la Cordillera occidental del Ecuador entre 08–s18N, escala 1/200.000. British Geological Survey-CODIGEM, Dirección Nacional de Geología, Quito.

Boyle, R. W. (1969). Hydrothermal transport and deposition of gold. *Economic Geology*, 64(1), 112–115. <https://doi.org/10.2113/gsecongeo.64.1.112>

Buiter, S. J. H., & Torsvik, T. H. (2014). A review of Wilson Cycle plate margins: A role for mantle plumes in continental break-up along sutures? *Gondwana Research*, 26(2), 627–653. <https://doi.org/10.1016/j.gr.2014.02.007>

Cabri, L. J., Newville, M., Gordon, R. A., Crozier, E. D., Sutton, S. R., McMahon, G., & Jiang, D. T. (2000). Chemical speciation of gold in arsenopyrite. *Canadian Mineralogist*, 38(5), 1265–1281. <https://doi.org/10.2113/gscanmin.38.5.1265>

Calvo G, Johnston A (2014) Curipamba Project - El Domo Deposit

Candela, P. A. 2004. Ores in the Earth's crust. *Treatise on Geochemistry*, 3, 411–431.
 Cediel, F. (2019). Phanerozoic orogens of northwestern South America: Cordilleran-type orogens. taphrogenic tectonics. the maracaibo orogenic float. The chocó-Panamá indenter. In *Frontiers in Earth Sciences*. https://doi.org/10.1007/978-3-319-76132-9_1

Chen, Y. W., Wu, J., & Suppe, J. (2019). Southward propagation of Nazca subduction along the Andes. *Nature*, 565(7740), 441–447. <https://doi.org/10.1038/s41586-018-0860-1>

Chew, D. M., Cardona, A., & Mišković, A. (2011). Tectonic evolution of western Amazonia from the assembly of Rodinia to its break-up. *International Geology Review*, 53(11–12), 1280–1296. <https://doi.org/10.1080/00206814.2010.527630>

Chiaradia M, Fontboté L (2001) Radiogenic lead signatures in Au-rich volcanic-hosted massive sulfide ores and associated volcanic rocks of the Early Tertiary Macuchi island arc (Western Cordillera of Ecuador). *Econ Geol* 96:1361–1378

Chiaradia, M., Plata, L., & Patino, E. (2003). *Geological setting , mineralogy , and*

geochemistry of the Early Tertiary Au-rich volcanic-hosted massive sulfide deposit of La Plata (Western. August, 13–16.

- Chiaradia, M., Fontboté, L., & Beate, B. (2004a). Cenozoic continental arc magmatism and associated mineralization in Ecuador. *Mineralium Deposita*, 39(2), 204–222. <https://doi.org/10.1007/s00126-003-0397-5>
- Chiaradia, M., Fontboté, L., & Paladines, A. (2004b). Metal sources in mineral deposits and crustal rocks of Ecuador (1° N–4° S): A lead isotope synthesis. *Economic Geology*, 99(6), 1085–1106. <https://doi.org/10.2113/gsecongeo.99.6.1085>
- Chiaradia M, Tripodi D, Fontboté L, Reza B (2008) Geologic setting, mineralogy, and geochemistry of the Early Tertiary Au-rich volcanic-hosted massive sulfide deposit of La Plata, Western Cordillera, Ecuador. *Econ Geol* 103:161–183
- Chiaradia, M., Muntener, O. M., & Beate, B. (2014). Quaternary sanukitoid-like andesites generated by intracrustal processes (Chacana caldera complex, Ecuador): Implications for archean sanukitoids. *Journal of Petrology*, 55(4), 769–802. <https://doi.org/10.1093/petrology/egu006>
- Cochrane R, Spikings R, Gerdes A, Ulianov A, Mora A, Villagómez D, Putlitz B, Chiaradia M (2014) Permo-Triassic anatexis, continental rifting and the disassembly of western Pangaea. *Lithos* 190–191: 383–402
- Colpron, M., Nelson, J. L., & Murphy, D. C. (2007). Northern Cordilleran terranes and their interactions through time. *GSA today*, 17(4/5), 4.
- Cordani, U. G., Fraga, L. M., Reis, N., Tassinari, C. C. G., & Brito-Neves, B. B. (2010). On the origin and tectonic significance of the intra-plate events of Grenvillian-type age in South America: A discussion. *Journal of South American Earth Sciences*, 29(1), 143–159. <https://doi.org/10.1016/j.jsames.2009.07.002>
- Cuenca, A. M. K. (2018). Cálculo de los recursos minerales del sulfuro masivo volcanogénico del depósito VMS El Domo, ubicado en la provincia de Bolívar. *Universidad Central del Ecuador*, 128. <http://www.ncbi.nlm.nih.gov/pubmed/7556065> <http://www.pubmedcentral.nih.gov/articlerender.fcgi?artid=PMC394507> <https://doi.org/10.1016/j.humphath.2017.05.005> <https://doi.org/10.1007/s00401-018-1825-z> <http://www.ncbi.nlm.nih.gov/pubmed/27157931>
- Davies, J. H. F. L., Marzoli, A., Bertrand, H., Youbi, N., Ernesto, M., & Schaltegger, U. (2017). End-Triassic mass extinction started by intrusive CAMP activity. *Nature communications*, 8(1), 1–8.
- Diamond, L. W. (1990). Fluid inclusion evidence for PVTX evolution of hydrothermal solutions in late-Alpine gold-quartz veins at Brusson, Val d'AYas, Northwest Italian Alps. *American Journal of Science*, 290(8), 912–958.

- Dubé B, Gosselin P, Mercier-Langevin P, Hannington M, Galley A (2007) Gold-rich volcanogenic massive sulphide deposits. In Goodfellow WD (ed) Mineral deposits of Canada: a synthesis of major deposit-types, district metallogeny, the evolution of geological provinces, and exploration methods, Geological Association of Canada, Mineral Deposits Division, Special Publication 5, pp 75–94
- Dubé, B., Gosselin, P., Mercier-Langevin, P., Hannington, M., & Galley, A. (2007). Gold-rich volcanogenic massive sulphide deposits. *Geological Association of Canada, Mineral Deposits Division*, 75-94.
- Eckstrand, O.R., Sinclair, W.D., and Thorpe, R.I., eds. 1995, *Geology of Canadian Mineral Deposit Types*, Geology of Canada, No. 8, Decade of North American Geology (DNAG): Geological Society of America, Part 1, p. 183-196.
- Eguez, A., 1986. Evolution Cenozoique de la Cordillere Occidentale Septentrionale d'Équateur: Les mineralisation associees. Unpublished PhD thesis; Universite Pierre et Marie Curie, Paris.
- Egüez, A.; Bourgois, J. (1986). La Formacion Apagua, edad y posición estructural en la Cordillera Occidental del Ecuador. In Cuarto Congreso Ecuatoriano de Geología Minas y Petroleos; Escuela Politecnica Nacional (eds.): Quito, Ecuador, 1986; pp. 161–178
- Fougerouse, D. (27 de June de 2021). *theconversation*. Obtenido de theconversation: <https://theconversation.com/not-so-foolish-after-all-fools-gold-contains-a-newly-discovered-type-of-real-gold-161819?fbclid=IwAR1LteOEEYU5bArzK5F150pwhZo7shtkY8ITJ1u5v5w6T764dZxzmGnZrdM>
- Frank, M. R., Simon, A. C., Pettke, T., Candela, P. A., & Piccoli, P. M. (2011). Gold and copper partitioning in magmatic-hydrothermal systems at 800°C and 100MPa. *Geochimica et Cosmochimica Acta*, 75(9), 2470–2482. <https://doi.org/10.1016/j.gca.2011.02.012>
- Franklin, J.M., Hannington, M.D., Jonasson, I.R., and Barrie, C.T., 1998, Arc-related volcanogenic massive sulphide deposits: Proceedings of Short Course on Metallogeny of Volcanic Arcs, January 24-25, Vancouver: British Columbia Geological Survey Open-File 1998-8, p. N1-N32
- Franklin, J.M., Sangster, D.M., and Lydon, J.W. (1981). Volcanic-associated massive sulfide deposits. Skinner, B.J., ed., *Economic Geology Seventy-fifth Anniversary Volume*: Economic Geology Publishing Company. <https://pubs.usgs.gov/bul/b1693/html/bull0bfp.htm>

- Frutos, J. (1982). Andean metallogeny related to the tectonic and petrologic evolution of the Cordillera. Some remarkable points. In *Ore Genesis* (pp. 493-507). Springer, Berlin, Heidelberg.
- Galley AG, Hannington MD, Jonasson IR (2007) Volcanogenic massive sulphide deposits. In Goodfellow WD (ed) *Mineral Deposits of Canada: A Synthesis of Major Deposit-Types, District Metallogeny, the Evolution of Geological Provinces, and Exploration Methods*, Geological Association of Canada, Mineral Deposits Division, Special Publication 5, pp 141–161
- Garrels, R. M. (1968). *Hydrothermal Transport and Deposition of Gold mole. 63*, 622–635.
- Hager, J. P., & Hill, R. B. (1970). Thermodynamic properties of the vapor transport reactions in the Au-Cl system by a transpiration-mass spectrometric technique. *Metallurgical Transactions*, 1(10), 2723–2731. <https://doi.org/10.1007/BF03037807>
- Hamilton, W.B., 1995, Subduction systems and magmatism: Geological Society of London Special Publication, v. 81, p. 3-28.
- Hannington, M. D., Poulsen, K. H., & Thomsen, J. F. (1999). Volcanogenic gold in the massive sulfide environment. Society of Economic Geologists.
- Hanley, J. J., & Gladney, E. R. (2011). The presence of carbonic-dominant volatiles during the crystallization of sulfide-bearing mafic pegmatites in the North Roby Zone, Lac des Iles Complex, Ontario. *Economic Geology*, 106(1), 33-54.
- Hedenquist, J. W., & Lowenstern, J. B. (1994). The role of magmas in the formation of hydrothermal ore deposits. In *Nature* (Vol. 370, Issue 6490, pp. 519–527). <https://doi.org/10.1038/370519a0>
- Heinrich, C. A., Günther, D., Audétat, A., Ulrich, T., & Frischknecht, R. (1999). Metal fractionation between magmatic brine and vapor, determined by microanalysis of fluid inclusions. *Geology*, 27(8), 755–758. [https://doi.org/10.1130/0091-7613\(1999\)027<0755:MFBMBA>2.3.CO;2](https://doi.org/10.1130/0091-7613(1999)027<0755:MFBMBA>2.3.CO;2)
- Herrington RJ, Zaykov VV, Maslennikov VV, Brown D, Puchkov VN (2005b) Mineral deposits of the Urals and links to geodynamic evolution. In: Hedenquist JW, Thompson JFH, Goldfarb RJ, Richards JR (eds) *Economic geology one hundredth anniversary volume 1905-2005.*, pp 1069–1095.
- Hughes, R. A., & Pilatasig, L. F. (2002). Cretaceous and Tertiary terrane accretion in the Cordillera Occidental of the Andes of Ecuador. *Tectonophysics*, 345(1–4), 29–48. [https://doi.org/10.1016/S0040-1951\(01\)00205-0](https://doi.org/10.1016/S0040-1951(01)00205-0)

- Hughes, R.; Bermudez, R. (1997). Geology of the Cordillera Occidental of Ecuador between 0°00' and 1°00' S. Proyecto de Desarrollo Minero y Control Ambiental, Programa de Información Cartográfica y Geológica; Report Number 4, 1st ed.; CODIGEM-BGS: Quito, Ecuador, 1997; p. 75.
- Hughes, R.A., Bermudez, R. & Espinel, G. (1998): Mapa geológico de la Cordillera Occidental del Ecuador entre 0°- 1°S, escala 1:200.000. CODIGEM- Ministerio de Energía y Minas- BGS publs., Quito, Nottingham
- Huston, D. L. (1992). Geologic and geochemical controls on the mineralogy and grain size of gold-bearing phases, eastern Australian volcanic-hosted massive sulfide deposits. *Economic Geology*, 87(3), 542–563. <https://doi.org/10.2113/gsecongeo.87.3.542>
- Huston, D. L. (2000). Gold in volcanic-hosted massive sulfide deposits: distribution, genesis, and exploration. *Reviews in Economic Geology*, 13, 401-426.
- Hutchinson, R.W., Spence, C.D., and Franklin, J.M., eds., 1982, Precambrian sulfide deposits, H.S. Robinson Memorial Volume: Geological Association of Canada Special Paper 25, 791 p.
- Ishihara, S., ed., 1974, Geology of the Kuroko deposits: Society of Mining Geologists of Japan, Special Issue 6, 473 p.
- Jaillard, E., Soler, P., Carlier, G. & Mourier, T. (1990). Geodynamic evolution of the northern and central Andes during early-to- middle Mesozoic times: a Tethyan model. *Journal of the Geological Society, London* 147, 1009-1022.
- Jaillard, E., Ordóñez, M., Suárez, J., Toro, J., Iza, D., & Lugo, W. (2004). Stratigraphy of the late Cretaceous-Paleogene deposits of the cordillera Occidental of central Ecuador: Geodynamic implications. *Journal of South American Earth Sciences*, 17(1), 49–58. <https://doi.org/10.1016/j.jsames.2004.05.003>
- James, S. E., & Hager, J. P. (1978). High Temperature Vaporization Chemistry in the Gold-Chlorine System Including Formation of Vapor Complex Species of Gold and Silver with Copper and Iron. *Metallurgical Transactions B*, 9(4), 501–508. <https://doi.org/10.1007/bf03321888>
- Johnston, A., & Calvo, G. (2014). *Curipamba project -El Domo deposit preliminary economic assessment central Ecuador*.
- Kaasalainen, H., & Stefánsson, A. (2011). Sulfur speciation in natural hydrothermal waters, Iceland. *Geochimica et Cosmochimica Acta*, 75(10), 2777–2791. <https://doi.org/10.1016/j.gca.2011.02.036>

- Kay, S.M., Mpodozis, C., Coira, B., 1999. Neogene magmatism, tectonism, and mineral deposits of the Central Andes (22° to 33°S latitude). In: Skinner, B.J. (Ed.), *Geology and Ore Deposits of the Central Andes. : Special Publication, No. 7.* Society of Economic Geologists, pp. 27–59.
- Kennan, L., & Pindell, J. L. (2009). Dextral shear, terrane accretion and basin formation in the Northern Andes: best explained by interaction with a Pacific-derived Caribbean Plate?. *Geological Society, London, Special Publications*, 328(1), 487-531.
- Kerr, A. (1997). Cretaceous Basaltic Terranes in Western Colombia: Elemental, Chronological and Sr-Nd Isotopic Constraints on Petrogenesis. *Journal of Petrology*, 38(6), 677–702. <https://doi.org/10.1093/petrology/38.6.677>
- Kerr, A. C., Aspden, J. A., Tarney, J. & Pilatasig, L. F. (2002). The nature and provenance of accreted oceanic blocks in western Ecuador: geochemical and tectonic constraints. *Journal of the Geological Society, London* 159, 577–594.
- Kouzmanov, K., & Pokrovski, G. S. (2020). Hydrothermal Controls on Metal Distribution in Porphyry Cu (-Mo-Au) Systems. In *Geology and Genesis of Major Copper Deposits and Districts of the World A Tribute to Richard H. Sillitoe* (Issue August). <https://doi.org/10.5382/sp.16.22>
- Landsberg, A. & Hoatson, C. L. (1970). The kinetics and equilibria of the gold-chloride system. *Journal of the Less-Common Metals*, 22, 327–339.
- Lentz, D. R., & Goodfellow, W. D. (1994). Petrology and geochemistry of altered volcanic and sedimentary rocks associated with the FAB stringer sulphide zone, Bathurst, New Brunswick. *Current Research, Geological Survey of Canada Paper*, 123-133.
- Litherland, M., Aspden, J.A. and Jemielita, R.A., (1994). The metamorphic belts of Ecuador. *Brit. Geol. Surv. Overseas Mem.*, 11, 147.
- Luzieux, L.D.A., Heller, F., Spikings, R., Vallejo, C.F. and Winkler, W., 2006. Origin and Cretaceous tectonic history of the coastal Ecuadorian forearc between 1N and 3S: paleomagnetic, radiometric and fossil evidence. *Earth Planet. Sci. Lett.*, 249, 400–414.
- Martin-Gombojav, N., & Winkler, W. (2008). Recycling of Proterozoic crust in the Andean Amazon Foreland of Ecuador: Implications for orogenic development of the Northern Andes. *Terra Nova*, 20(1), 22–31. <https://doi.org/10.1111/j.1365-3121.2007.00782.x>
- McClenaghan, S. H., Lentz, D. R., Martin, J., & Diegor, W. G. (2009). Gold in the Brunswick No. 12 volcanogenic massive sulfide deposit, Bathurst Mining Camp, Canada: Evidence from bulk ore analysis and laser ablation ICP-MS data on

- sulfide phases. *Mineralium Deposita*, 44(5), 523–557.
<https://doi.org/10.1007/s00126-009-0233-7>
- Mercier-Langevin, P., Hannington, M. D., Dubé, B., & Bécu, V. (2011). The gold content of volcanogenic massive sulfide deposits. *Mineralium Deposita*, 46(5), 509–539. <https://doi.org/10.1007/s00126-010-0300-0>
- Migdisov, A. A., & Bychkov, A. Y. (1998). The behaviour of metals and sulphur during the formation of hydrothermal mercury-antimony-arsenic mineralization, Uzon caldera, Kamchatka, Russia. *Journal of Volcanology and Geothermal Research*, 84(1–2), 153–171. [https://doi.org/10.1016/S0377-0273\(98\)00038-9](https://doi.org/10.1016/S0377-0273(98)00038-9)
- Mikucki, E. J. (1998). Hydrothermal transport and depositional processes in Archean lode-gold systems: A review. *Ore Geology Reviews*, 13(1-5), 307-321.
- Noble, S.R., Aspden, J.A. and Jemielita, R., (1997). Northern Andean crustal evolution: New U-Pb geochronological constraints from Ecuador. //Bull. Geol. Soc. Am.//, 109, 789–798.
- Nordstrom, D. K., Cunningham, K. M., Ball, J. W., Xu, Y., & Schoonen, M. A. A. (1998). Sulfur redox chemistry and the origin of thiosulfate in hydrothermal waters of Yellowstone National Park. *Water-Rock Interact., Proc. Int. Symp., 9th*, 62(23), 641–644.
- Ohmoto, H., and Skinner, B.J., eds., 1983, The Kuroko and related volcanogenic massive sulfide deposits: Economic Geology, Monograph 5, 604 p.
- Palenik, C. S., Utsunomiya, S., Reich, M., Kesler, S. E., Wang, L., & Ewing, R. C. (2004). “Invisible” gold revealed: Direct imaging of gold nanoparticles in a Carlin-type deposit. *American Mineralogist*, 89(10), 1359–1366.
<https://doi.org/10.2138/am-2004-1002>
- Palyanova, G. A., Laptev Yu, V., & Kolonin, G. R. (1993). An experimental study of gold mobility in sulphur-saturated solutions in connection with conditions of gold-containing sulphide-rich assemblages. In *Proceedings of II Biennial SGA Meeting “Current Research in Geology Applied to Ore Deposits”*. Granada, Spain (pp. 527-530).
- Pardo-Trujillo, A., Cardona, A., Giraldo, A. S., León, S., Vallejo, D. F., Trejos-Tamayo, R., Plata, A., Ceballos, J., Echeverri, S., Barbosa-Espitia, A., Slattery, J., Salazar-Ríos, A., Botello, G. E., Celis, S. A., Osorio-Granada, E., & Giraldo-Villegas, C. A. (2020). Sedimentary record of the Cretaceous–Paleocene arc–continent collision in the northwestern Colombian Andes: Insights from stratigraphic and provenance constraints. *Sedimentary Geology*, 401.
<https://doi.org/10.1016/j.sedgeo.2020.105627>

- Piercey, S. J. (2011). The setting, style, and role of magmatism in the formation of volcanogenic massive sulfide deposits. *Mineralium Deposita*, 46(5), 449–471. <https://doi.org/10.1007/s00126-011-0341-z>
- Phillips, G. N., & Evans, K. A. (2004). Role of CO₂ in the formation of gold deposits. *Nature*, 429(6994), 860–863.
- Pokrovski, G. S., Akinfiyev, N. N., Borisova, A. Y., Zotov, A. V., & Kouzmanov, K. (2014). Gold speciation and transport in geological fluids: Insights from experiments and physical-chemical modelling. *Geological Society Special Publication*, 402(1), 9–70. <https://doi.org/10.1144/SP402.4>
- Pokrovski, G. S., Borisova, A. Y., & Harrichoury, J. C. (2008). The effect of sulfur on vapor-liquid fractionation of metals in hydrothermal systems. *Earth and Planetary Science Letters*, 266(3–4), 345–362. <https://doi.org/10.1016/j.epsl.2007.11.023>
- Pokrovski, G. S., Tagirov, B. R., Schott, J., Bazarkina, E. F., Hazemann, J. L., & Proux, O. (2009). An in situ X-ray absorption spectroscopy study of gold-chloride complexing in hydrothermal fluids. *Chemical Geology*, 259(1–2), 17–29. <https://doi.org/10.1016/j.chemgeo.2008.09.007>
- Pokrovski, G. S., Zakirov, I. V., Roux, J., Testemale, D., Hazemann, J. L., Bychkov, A. Y., & Golikova, G. V. (2002). Experimental study of arsenic speciation in vapor phase to 500°C: Implications for As transport and fractionation in low-density crustal fluids and volcanic gases. *Geochimica et Cosmochimica Acta*, 66(19), 3453–3480. [https://doi.org/10.1016/S0016-7037\(02\)00946-8](https://doi.org/10.1016/S0016-7037(02)00946-8)
- Poulsen KH, Hannington MD (1996) Volcanic-associated massive sulphide gold. In Eckstrand RO, Sinclair WD, Thorpe RI (eds) *Geology of Canadian Mineral Deposit Types: Geological Society of America, DNAG*, v. P-1. *Geology of Canada* 8:183–196
- Poulsen KH, Robert F, Dubé B (2000) Geological classification of Canadian gold deposits. *Bull-Geol Surv Can* 540:106
- Pratt, W. (2008). Las Naves Project, Bolívar, Ecuador. PRODEMINCA.
- Pratt, W. T., Figueroa, J. F., Flores, B. G. (1997): Mapa geológico de la Cordillera Occidental del Ecuador entre 3°- 4°S. escala 1/200.000. CODIGEM- Min. Energ. Min.- BGS publs., Quito.
- Prokin VA, Buslaev FP (1999) Massive copper-zinc sulphide deposits in the Urals. *Ore Geol Rev* 14:1–69
- Quisefit, J. P., Toutain, J. P., Bergametti, G., Javoy, M., Cheynet, B., & Person, A. (1989). Evolution versus cooling of gaseous volcanic emissions from Momotombo Volcano, Nicaragua: Thermochemical model and observations. *Geochimica et Cosmochimica Acta*, 53(10), 2591–2608. <https://doi.org/10.1016/0016->

7037(89)90131-2

- Ramos, V.A. and Aleman, A., 2000. Tectonic evolution of the Andes. In: Tectonic Evolution of South America (U. Cordani, E.J. Milani, A. Thomaz Filho and M.C. Campos Neto, eds), pp. 635–685. Institut de recherche pour le de veloppement, Rio de Janeiro.
- Reich, M., Kesler, S. E., Utsunomiya, S., Palenik, C. S., Chryssoulis, S. L., & Ewing, R. C. (2005). Solubility of gold in arsenian pyrite. *Geochimica et Cosmochimica Acta*, 69(11), 2781–2796. <https://doi.org/10.1016/j.gca.2005.01.011>
- Resources, Largo. largoresources. [On line] Largo Resources Ltd., October 16 of 2006. [Quoted on: 08 de Agust de 2021.] <https://www.largoresources.com/English/news-and-media/news-details/2006/Largo-Resources-Options-Macuchi-VMS-Property-in-Ecuador-to-Aur-Resources/default.aspx>.
- Richards JP (2003) Tectono-magmatic precursors for porphyry Cu- (Mo-Au) deposit formation. *Econ Geol* 98:1515–1533
- Richards, J. P. (2011). Magmatic to hydrothermal metal fluxes in convergent and collided margins. *Ore Geology Reviews*, 40(1), 1–26. <https://doi.org/10.1016/j.oregeorev.2011.05.006>
- Saunders, A.D., Tarney, J., Kerr, A.C., Kent, R.W., (1996). The formation and fate of large igneous provinces. *Lithos* 37, 81–95.
- Saunders, J. A., & Schoenly, P. A. (1995). Boiling, colloid nucleation and aggregation, and the genesis of bonanza Au-Ag ores of the Sleeper deposit, Nevada. *Mineralium Deposita*, 30(3-4), 199-210.
- Savoyat, F.; Vernet, R.; Sigal, J.; Mosquera, C.; Granja, J.; Guevara, G. (1970). Formaciones Sedimentarias de la Sierra Tectonica Andina del Ecuador; Servicio Nacional de Geologia y Minería—Institut Francais du Petrole; 1970; unpublished report.
- Scaini, M. J., Bancroft, G. M., & Knipe, S. W. (1998). Reactions of aqueous Au¹⁺ sulfide species with pyrite as a function of pH and temperature. *American Mineralogist*, 83(3–4), 316–322. <https://doi.org/10.2138/am-1998-3-415>
- Schandl ES (2009) Petrographic and Mineralogical Study of the Shanks, W.C. Pat, III, and Thurston, Roland, eds., 2012, Volcanogenic massive sulfide occurrence model: U.S. Geological Survey Scientific Investigations Report 2010–5070–C, 345 p.
- Sillitoe RH (1972) A plate tectonic model for the origin of porphyry copper deposits. *Econ Geol* 67:184–197

- Sillitoe, R. H., Hannington, M. D., & Thompson, J. F. (1996). High sulfidation deposits in the volcanogenic massive sulfide environment. *Economic geology*, *91*(1), 204-212.
- Schutte, P. (2010). *Geochronology , geochemistry , and isotopic composition (Sr , Nd , Pb) of Tertiary porphyry systems in Ecuador Université de Genève Département de Minéralogie faculté des sciences Prof . Urs Schaltegger Dr . Massimo Chiaradia Geochronology , Geochemistr.*
- Schütte, P., Chiaradia, M., Barra, F., Villagómez, D., & Beate, B. (2012). Metallogenic features of Miocene porphyry Cu and porphyry-related mineral deposits in Ecuador revealed by Re-Os, ⁴⁰Ar/ ³⁹Ar, and U-Pb geochronology. *Mineralium Deposita*, *47*(4), 383–410. <https://doi.org/10.1007/s00126-011-0378-z>
- Scotney, P. M., Roberts, S., Herrington, R. J., Boyce, A. J., & Burgess, R. (2005). The development of volcanic hosted massive sulfide and barite-gold ore bodies on Wetar Island, Indonesia. *Mineralium Deposita*, *40*(1), 76–99. <https://doi.org/10.1007/s00126-005-0468-x>
- Seo, J. H., Guillong, M., & Heinrich, C. A. (2009). The role of sulfur in the formation of magmatic-hydrothermal copper-gold deposits. *Earth and Planetary Science Letters*, *282*(1–4), 323–328. <https://doi.org/10.1016/j.epsl.2009.03.036>
- Sewell, D. M., & Wheatley, C. J. V. (1994). The Lerokis and Kali Kuning submarine exhalative gold-silver-barite deposits, Wetar Island, Maluku, Indonesia. *Journal of Geochemical Exploration*, *50*(1–3), 351–370. [https://doi.org/10.1016/0375-6742\(94\)90031-0](https://doi.org/10.1016/0375-6742(94)90031-0)
- Shanks, W.C.P., III, and Thurston, R., eds., 2012, Volcanogenic Massive Sulfide Occurrence Model: U.S. Geological Survey Scientific Investigations Report, v. 2010-5070-C, p. 345.
- Sillitoe, R. H. (2010). Porphyry copper systems. *Economic Geology*, *105*(1), 3–41. <https://doi.org/10.2113/gsecongeo.105.1.3>
- Sillitoe, R. H., Hannington, M. D., & Thompson, J. F. H. (1996). High sulfidation deposits in the volcanogenic massive sulfide environment. *Economic Geology*, *91*(1), 204–212. <https://doi.org/10.2113/gsecongeo.91.1.204>
- Simon, A. C., Frank, M. R., Pettke, T., Candela, P. A., Piccoli, P. M., & Heinrich, C. A. (2005). Gold partitioning in melt-vapor-brine systems. *Geochimica et Cosmochimica Acta*, *69*(13), 3321–3335. <https://doi.org/10.1016/j.gca.2005.01.028>
- Simon, G., Huang, H., Penner-Hahn, J. E., Kesler, S. E., & Kao, L. S. (1999). Oxidation state of gold and arsenic in gold-bearing arsenian pyrite. *American Mineralogist*, *84*(7–8), 1071–1079. <https://doi.org/10.2138/am-1999-7-809>

- Sinton, C.W., Duncan, R.A., Storey, M., Lewis, J., Estrada, J.J., 1998. An oceanic flood basalt province within the Caribbean Plate. *Earth Planet. Sci. Lett.* 155, 221–235
- Spikings RA, Cochrane RS, Villagómez D, Van der Lelij D, Vallejo C, Winkler W, Beate B (2015) The geological history of north Western South America: from Pangaea to the early collision of the Caribbean Large Igneous Province (290–75 Ma). *Gond, Res.* 27:95–139
- Spikings, R. A., Winkler, W., Hughes, R. A. & Handler, R. (2005). Thermochronology of allochthonous terranes in Ecuador: unravel- ling the accretionary and post- accretionary history of the Northern Andes. *Tectonophysics* 399, 195-220.
- Spikings, R.A., Winkler, W., Seward, D. and Handler, R., (2001). Along-strike variations in the thermal and tectonic response of the continental Ecuadorian Andes to the collision with heteroge- neous oceanic crust. *Earth Planet. Sci. Lett.*, 186, 57–73.
- Teixeira, W., Tassinari, C. C. G., Cordani, U. G., & Kawashita, K. (1989). A review of the geochronology of the Amazonian Craton: Tectonic implications. *Precambrian Research*, 42(3–4), 213–227. [https://doi.org/10.1016/0301-9268\(89\)90012-0](https://doi.org/10.1016/0301-9268(89)90012-0)
- Tomkins, A. G. (2010). Windows of metamorphic sulfur liberation in the crust: Implications for gold deposit genesis. *Geochimica et Cosmochimica Acta*, 74(11), 3246–3259. <https://doi.org/10.1016/j.gca.2010.03.003>
- Toussaint, J. F., & Restrepo, J. J. (1994). The Colombian Andes During Cretaceous Times. *Cretaceous Tectonics of the Andes*, 61–100. https://doi.org/10.1007/978-3-322-85472-8_2
- Usher, A., McPhail, D. C., & Brugger, J. (2009). A spectrophotometric study of aqueous Au(III) halide-hydroxide complexes at 25–80 °C. *Geochimica et Cosmochimica Acta*, 73(11), 3359–3380. <https://doi.org/10.1016/j.gca.2009.01.036>
- Vallance, J., Markowski, A., Fontboté, L., and Chiaradia, M., 2003, Miner- alogical and fluid inclusion constraints on the genesis of gold-skarn deposits in the Nambija district (Ecuador), in Eliopoulos, D., et al., eds., Mineral ex- ploration and sustainable development: Rotterdam, Millpress, p. 399–402.
- Vallance, J., Fontboté, L., Chiaradia, M., Markowski, A., Schmidt, S., & Vennemann, T. (2009). Magmatic-dominated fluid evolution in the Jurassic Nambija gold skarn deposits (southeastern Ecuador). *Mineralium Deposita*, 44(4), 389–413. <https://doi.org/10.1007/s00126-009-0238-2>
- Vallejo, C., Spikings, R.A., Luzieux, L., Winkler, W., Chew, D., Page, L., (2006): The early interaction be- tween the Caribbean Plateau and the NW South American Plate. *Terra Nova* 18, 264–269

- Vallejo, C.F. (2007). Evolution of the Western Cordillera in the Andes of Ecuador (Late Cretaceous Paleogene). Ph.D. Thesis, ETH Zürich, Zürich, Switzerland, 2007.
- Vallejo C, Winkler W, Spikings RA, Luzieux L, Heller F, Bussy F (2009) Mode and timing of terrane accretion in the forearc of the Andes in Ecuador. In: Kay SM, Ramos VA, Dickinson WR (eds.), Backbone of the Americas: Shallow Subduction, Plateau Uplift, and Ridge and Terrane Collision. Geol Soc Am Memoir 204
- Vallejo, C., Soria, F., Tornos, F., Naranjo, G., Rosero, B., Salazar, F., & Cochrane, R. (2016). Geology of El Domo deposit in central Ecuador: a VMS formed on top of an accreted margin. *Mineralium Deposita*, 51(3), 389–409. <https://doi.org/10.1007/s00126-015-0616-x>
- Vallejo, C., Spikings, R. A., Horton, B. K., Luzieux, L., Romero, C., Winkler, W., & Thomsen, T. B. (2019). Late cretaceous to Miocene stratigraphy and provenance of the coastal forearc and Western Cordillera of Ecuador: Evidence for accretion of a single oceanic plateau fragment. In *Andean Tectonics*. Elsevier Inc. <https://doi.org/10.1016/b978-0-12-816009-1.00010-1>
- Vallejo, C., Almagor, S., Romero, C., Herrera, J. L., Escobar, V., Spikings, R. A., Winkler, W., & Vermeesch, P. (2020). Sedimentology, provenance and radiometric dating of the Silante Formation: Implications for the Cenozoic evolution of the Western Andes of Ecuador. *Minerals*, 10(10), 1–31. <https://doi.org/10.3390/min10100929>
- Van Der Lelij, R., Spikings, R. A., Kerr, A. C., Kounov, A., Cosca, M., Chew, D., & Villagomez, D. (2010). Thermochronology and tectonics of the Leeward Antilles: Evolution of the southern Caribbean Plate boundary zone. *Tectonics*, 29(6). <https://doi.org/10.1029/2009TC002654>
- van der Lelij, R., Spikings, R., Ulianov, A., Chiaradia, M., & Mora, A. (2016). Palaeozoic to Early Jurassic history of the northwestern corner of Gondwana, and implications for the evolution of the Iapetus, Rheic and Pacific Oceans. *Gondwana Research*, 31, 271–294. <https://doi.org/10.1016/j.gr.2015.01.011>
- Velásquez, G., Béziat, D., Salvi, S., Siebenaller, L., Borisova, A. Y., Pokrovski, G. S., & De Parseval, P. (2014). Formation and deformation of pyrite and implications for gold mineralization in the El Callao District, Venezuela. *Economic Geology*, 109(2), 457–486. <https://doi.org/10.2113/econgeo.109.2.457>
- Vera R., (2016). Geology of Ecuador: Gráficas Iberia, second edition, 154p., Quito.
- Villagómez, D., Spikings, R., Magna, T., Kammer, A., Winkler, W., Beltrán, A., 2011. Geochronology, geochemistry and tectonic evolution of the Western and Central cordilleras of Colombia. *Lithos* 125, 875–896.
- Vlassopoulos, D., Wood, S. A., & Mucci, A. (1990). Gold speciation in natural waters:

II. The importance of organic complexing-experiments with some simple model ligands. *Geochimica et Cosmochimica Acta*, 54(6), 1575–1586. [https://doi.org/10.1016/0016-7037\(90\)90392-X](https://doi.org/10.1016/0016-7037(90)90392-X)

Williams-Jones, A. E., Bowell, R. J., & Migdisov, A. A. (2009). Gold in solution. *Elements*, 5(5), 281–287. <https://doi.org/10.2113/gselements.5.5.281>

Withjack, M. O., Schlische, R. W., & Olsen, P. E. (2002). Rift-basin structure and its influence on sedimentary systems.

Yang K, Scott SD (2003) Geochemical relationships of felsic magmas to ore metals in massive sulfide deposits of the Bathurst Mining Camp, Iberian Pyrite Belt, Hokuroku District, and the Abitibi Belt. In Goodfellow WD, McCutcheon SR, Peter JM (eds) Massive sulfide deposits of the Bathurst mining camp, New Brunswick, and northern Maine. Economic Geology Monograph 11.

Ziegler, P.L., 1992, Plate tectonics, plate moving mechanisms and rifting: Tectonophysics, v. 215, p. 9-34.